Stabilization analysis of the lumbar spine in autonomous vehicles

Anna Marbus
July 2022

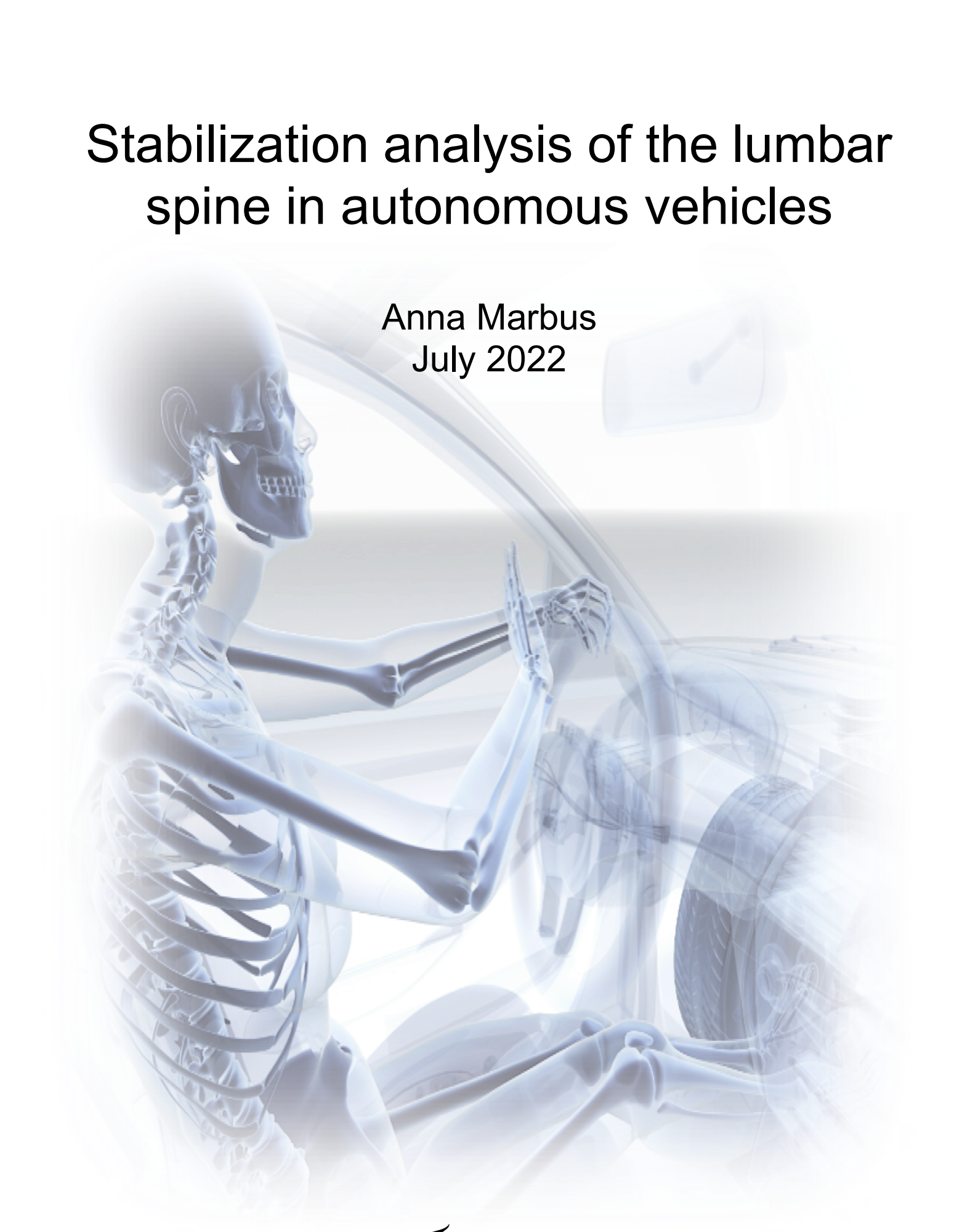

TU Delft

Lumbar stabilization analysis in autonomous vehicles

by

A. Marbus

to obtain the degree of Master of Science
at the Delft University of Technology,
to be defended publicly on Friday July 15, 2022 at 2:00 PM.

Student number:	4437381	
Project duration:	March 1, 2021 – July 1, 2022	
Thesis committee:	Dr. Ir. R. Happee,	TU Delft, supervisor
	Dr. Ir A. Seth,	TU Delft
	Dr. Ir. E. van der Kruk	TU Delft

This thesis is confidential and cannot be made public until July 15, 2022.

TU Delft

Preface

Before you lies my graduation project, containing the result of research conducted at Delft University of Technology. With this project I am able to fulfill the graduation requirements of the Master Biomedical Engineering.

As I was not a well-behaved high school student, I did not expect to get into Clinical Technology. Yet I had never felt so destined for a program before. Six years ago, against all odds, I embarked on this journey.

From the starting years, I noticed developing an increased interest in control theory and an interest in the field of neurology. As a consequence, I decided to pursue a Master in Biomedical Engineering with a discipline in neuromusculoskeletal biomechanics. Therefore, I decided to perform my graduation project in the (sub)field of my greatest interest. I started working with OpenSim for the first time and aimed to enhance a neuromusculoskeletal model to simulate car-passenger interaction. Current project has been very educational. The associated model development was quite challenging. However, I am proud of the end result and I hope you enjoy reading my report.

The graduation research was conducted under the supervision of Riender Happee and I would like to thank him for the support and the good help. I would like to thank Ajay Seth for his guidance throughout the process.

Besides my supervisors, I would like to express my gratitude towards my parents and friends for their endless support over the years. Thank you for the constant appreciation and the ability to clear my mind around you.

You may insinuate this thesis concludes my journey as a student. However, I am not ready to give up studying. I developed a highly interest in human-machine interaction and therefore, I decided to pursue a master in Robotics. I want to learn all about how people and automated systems interact with each other. That being the case, I have to graduate all over again and hopefully I am able to write you yet another preface in two years.

A. Marbus
Leiden, June 2022

Summary

The objective of this study is to simulate lumbar stabilization in autonomous vehicles through the utility of OpenSim. Considering sufficient isometric strength is required for dynamic analysis, validity of the full-body model developed by Schmid et al. [43] in isometric conditions is examined first. This encompasses the establishment of maximal isometric force exterted by the trunk in sagittal and frontal plane. The model is solved using an inverse-dynamics based static optimization and the model-predicted strength was taken to be the highest external force for which the *Static Optimization Tool* successfully solved [46]. Finally, isometric model conditions are validated against literature. Predicted strength correlated within 1 standard deviation (SD) of the in vivo measurements and therefore, yielded realistic results in forward, rearward and lateral direction.

After validating isometric conditions, dynamic stabilization of the spine and trunk while seated, are predicted. The goal of the dynamic analysis is to investigate how intrinsic and extrinsic properties contribute to lumbar stabilization as a function of pelvis translations. As a consequence, intrinsic and extrinsic properties are embedded in the OpenSim model from Schmid et al. [43].

Forward simulations of car-passenger interactions are generated in sagittal plane and validated using existing data with erect posture and unsupported back. However, aforementioned model is quite complex and as a consequence, operating forward simulations are demanding. Therefore, model adjustments, designed to meet the needs of dynamic simulation, are made. Thereupon, contemporary study investigates in what way implemented muscles are qualified to stabilize the lumbar spine in company of isometric thorax loads. Subsequently, contribution of intrinsic and extrinsic properties are explored. This symbolizes that effects of feedback loops and co-contraction are scrutinized. Thereupon, by dint of Gauss-Newton optimization scheme, extrinsic muscle properties are fitted to experimental data. In the fullness of time, lumbar bending, evoked by a translational force disturbance, is compared with experimental outcomes.

Conclusively, isometric model predictions correlated highly with in vivo data, indicating suitability for the accurate prediction of maximal trunk muscle strength. Dynamic analysis elucidated contribution of intrinsic and extrinsic properties. The model reproduced experimentally observed lumbar kinematics with reasonable fits in time and frequency domain. Further research is, nonetheless, needed to validate and complement the current study.

Contents

List of Figures

List of Tables

List of Abbreviations

CE	Contractile element
COG	Center of gravity
COM	Center of mass
DOF	Degrees of freedom
EMG	Electromyography
FRF	Frequency response function
NMS	Neuromusculoskeletal system
PE	Parallel element
SD	Standard deviation
SE	Serial element
VAF	Variance accounted for

1 Introduction

In this chapter, the background of the project will be introduced which will inform the reader briefly about the project topic in general. Before moving into the problem analysis, which will justify the research objectives, the research questions are stated and the project scope will be defined. At the end of this chapter, the used methodologies for answering the research questions are made clear.

1.1. Background

Since there is no longer the need to drive, automated cars have the benefit of freeing time for the driver. This situation pioneers for new seating inclination since the driver is no longer forced to sit behind the steering wheel. To adapt the vehicle's interior for this new way of driving, comprehension of how users would like to sit in automated cars is desired.

The driving position is presented by non-neutral spinal postures [31]. Generally, a reduction in lumbar lordosis and an increased or decreased neck flexion is adopted. The problem of attribution is concerned with identifying perturbations of autonomous vehicles causing discomfort. The minute a car starts moving and is subject to accelerations and decelerations, the driver experiences various forces, including up-and-down vibrations, as it sways from side to side. To resist mechanical perturbations and maintain equilibrium, the spine has to be stable. Stabilization is achieved by the postural control system which depends on intact sensory information to generate muscle reactions [28]. If the postural control system does not adjust appropriately, potential hazards for musculoskeletal tissue may arise [28]. Therefore, to improve postural control, a stable base of support is needed. Early studies on sitting posture reported a raised activation of low back muscles in absence of lumbar support [31]. Altered muscle activation may be attributed by two main factors: drivers maintain the same sitting position and due continuous changes in vehicle velocity adequately control posture is required. Hence, low back pain is frequently reported among drivers exposed to perturbations.

1.2. Motivation

Most research focuses on the technical aspects of the car. However, for acceptance by the general public, more insight into car-passenger interaction should be gained. Accordingly, there is a need to understand how movements of self-driving cars are transmitted to passengers and how passengers cope with perturbations affecting passenger's balance. By investigating changes in electromyography (EMG) signals, muscle activation can be inferred [24]. However, to gain better understanding what muscles are doing during driving or stabilization, a representation of the internal muscles is needed, which cannot be obtained with EMG measurements [41]. Hence, to come up with the estimation of internal forces caused by mechanical perturbations and to address optimal comfort in self-driving cars, musculoskeletal models have been introduced. To give an instance, Van Drunen et al. [10] experimentally validated a model capturing lumbar stabilization. Be that as it may, lumbar bending was modelled by only one degree of freedom (DOF). Additionally, Mirakhorlo et al. [32] simulated postural stabilization in vibration and dynamic driving. The model from Mirakhorlo et al. [32] included muscular stabilization in neck, arms and legs. Stabilization of the lumbar spine was, however, simplified by virtue of torque

generating actuators.

The objective of this project is to adjust and enhance a musculoskeletal model to such an extent that it can be used for isometric and dynamic analysis in a motion comfort study. Such a model will facilitate research and design related to postural stabilization in particular for seated car occupants. As outlined in the literature study, knowledge on lumbar stabilization as needed to develop such a model is currently lacking.

1.3. Research question

This study will use existing biomechanical data to address the following research questions

1. In what way are the implemented muscles able to stabilize the lumbar spine with isometric thorax loads?
2. How do feedback loops and muscle co-activation contribute to lumbar stabilization as a function of pelvis translations?

1.4. Goal and approach

The goal of this research is to generate simulation of the car-passenger interaction by using a neuro-musculoskeletal model. To achieve the indicated goal, a stepwise approach is followed (Fig. 1.1). The first step is to validate the model in isometric conditions. Hence, maximal isometric strength in sagittal and frontal plane is resolved. In the second step, structural and neural alterations are introduced in the model. In the third step, which includes simulation of dynamic stabilization, vehicle circumstances are simulated. Finally, dynamic validation is presented in time and frequency domain.

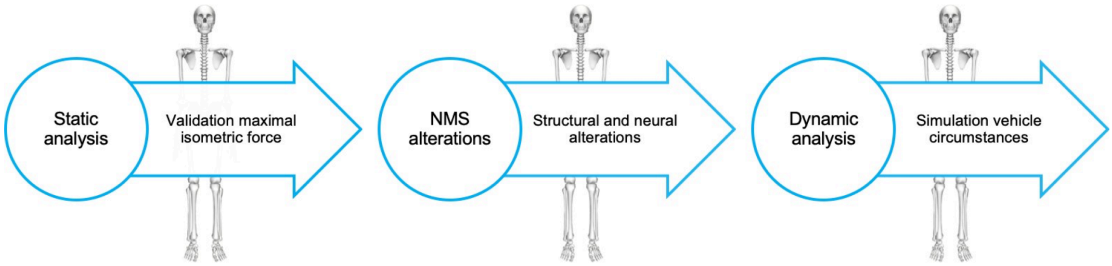

Figure 1.1: step-wise approach. Firstly, a static analysis is generated by using the NMS developed by Schmid et al. [43]. Secondly, structural and neural alterations are introduced in the NMS. Thirdly, vehicle circumstances are simulated and simulation of lumbar stabilization is generated.

2

Static analysis

To assess muscle strength, it is important to evaluate the model's isometric response. Isometric results serve as a control check considering sufficient isometric strength is required for dynamic analysis. Isometric measurements can be explored in sagittal, frontal and transverse planes. In this study, emphasis lies on sagittal and frontal planes. At the beginning of this chapter, a description of the musculoskeletal model is given. Thereafter, methodology of the static analysis is deliberated.

2.1. Neuromusculoskeletal model

The musculoskeletal model developed by Schmid et al. [43] provided the foundation for this research. Schmid et al. [43] constructed OpenSim-based musculoskeletal full-body models for children and adolescents aged 6–18 years. Schmid et al. [43] followed best practice guidelines for verification and validation of musculoskeletal models and sought to ensure pertinent musculoskeletal trunk strength and spinal loading in comparison to measured values. In the ongoing study, the OpenSim model of an 18-year old male is brought into play.

The model from Schmid et al. [43] holds 552 muscles and reserves 116-DOF. Furthermore, Schmid et al. [43] implemented 20 point actuators exerting an optimal force of 1000-N. Indicated actuators are applied to sternum and ribs and represent forces transmitted by costal cartilage. A portrait of the OpenSim model is observable in figure 2.1. A large number of muscles is exhibited. Point actuators are, on the contrary, not perceptible.

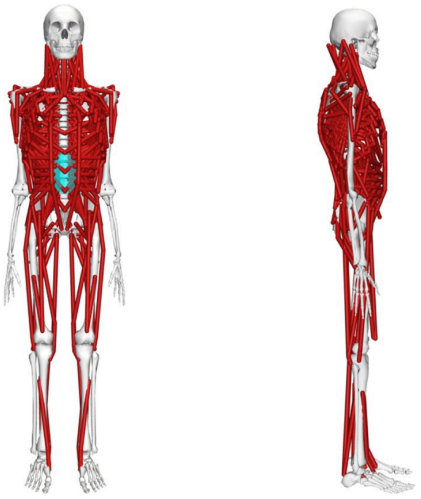

Figure 2.1: frontal and sagittal view of the musculoskeletal model developed by Schmid et al. [43]. The model possesses 552 muscles, 20 point actuators and retains 116-DOF.

2.1.1. Muscle model algorithm

In simulation studies, a muscle model is an algorithm transforming muscle activation into muscle force [5]. The model developed by Schmid et al. [43] incorporates the algorithm accredited by Thelen et al. [48]. Indicated algorithm utilizes a standard equilibrium muscle model based on the Hill model (Fig. 2.2). The Hill model typically consists of a contractile element (CE), a parallel element (PE) and a series element (SE). The CE represents aspects of active force production in response to excitation [4]. This force is embodied across the SE. The SE in the Hill muscle model acts elastically according to a force-extension relationship [22]. In this relationship the SE force, below its unloaded length, equals zero [4]. It is, however, important to mention that the SE force increases to gradually greater force when stretched to longer lengths beyond the unloaded length [22]. The SE is by definition undamped. Nonetheless, a small amount of damping could enhance the numerical efficiency and stability of the model [50]. The PE, on the contrary, is parallel to the CE. By using a function similar to the SE force-extension relationship, the PE gives rise to a force [48].

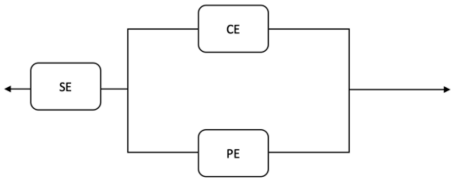

Figure 2.2: illustration of Hill muscle model comprising the contractile element (CE), the passive parallel element (PE) connected in parallel and the elastic element (SE) in series.

The muscle model compromises several constants. Each constant is assigned to the three aforementioned components of the muscle-tendon complex. Moreover, some constants may be equivalent for all muscles whereas other constants may vary between muscles. The following constants differ between muscles

- F_0^M, the maximum isometric force of the muscle (CE)
- l_0^M, the optimal fiber length of the muscle (CE)
- l_S^T, the tendon slack length (SE)
- α_0, the pennation angle of the muscle fibers at the optimal fiber length (CE and PE)

Dimensionless constants that are identical across muscles are

- ε_0^M = 0.60, passive muscle strain due to maximal isometric force (PE)
- k_t = 3.00, an exponential shape factor (SE)
- ε_0^T = 0.033, tendon strain due to maximal isometric force (SE)
- F_t^T = 0.33, normalized tendon force above which tendon force and tendon strain are linear (SE)
- k^{PE} = 4.00, an exponential shape factor for the passive force-length relationship (PE)
- γ = 0.50, a shape factor for the Gaussian active force-length relationship (CE)
- A_f = 0.30, a shape factor for the force-velocity relationship (CE)
- F_l^M = 1.80, maximum normalized muscle force achievable when the fiber is lengthening (CE)
- k_{lin} = 1.71/ε_0^T, a linear shape factor (SE)
- ε_t^T = 0.61/ε_0^T, tendon strain above which tendon force is linear with respect to tendon strain (SE)

2.2. Static Optimization Tool

The static analysis comprises three assessments: examining maximal isometric flexion and extension in sagittal plane and examining maximal isometric flexion in frontal plane. Static optimization is a method for resolving net joint moments into individual muscle forces [8][46]. The technique is called 'static' since calculations are performed at each time frame, without integrating the equations of motion between time steps [8][46].

Such a prediction is, however, challenging due to the non-uniqueness of the calculated muscle forces. On account of the fact that the model has more muscles than DOF, it is said to be redundant [38]. For that reason, an infinite number of possible muscle force solutions exist.

As a means to solve the redundancy problem, inverse dynamics solutions are constrained by prescribed model states [8][46]. Prescribed model states are described by generalized coordinates (q) and velocities ($\dot{q}$). Thereafter, muscle forces are resolved by minimizing the objective function, given by [46]

$$\sum_{n=1}^{m} (a_m)^p \tag{2.1}$$

where a_m represents the activation in m^{th} muscle and p constitutes a positive integer. Typically, an the sum of squared muscle activations (p = 2) is used for research applications.

Ultimately, the model-predicted strength is taken to be the highest external force for which the *Static Optimization Tool* successfully solved [46]. The *Static Optimization Tool* throws an exception at the instant constraints are violated. On that occasion, OpenSim suggests to append additional forces to reduce reported constraints. Accordingly, maximal isometric force of reported muscles is increased by incremental steps of 10-N. An overview, exhibiting exact alterations, is provided in Appendix A.

2.2.1. Maximal isometric force in sagittal plane

The *Static Optimization Tool* utilizes the disclosed motion of the model to solve the equations of motion for the undisclosed generalized forces [8][46]. The tool requires three input files: an OpenSim model, external load data and a motion file containing the time histories of generalized coordinates that describe the movement of the model [8][46]. For the static analysis, the model is constrained to static posture (q, $\dot{q} = 0$).

Conditions proposed in the in vivo experiment conducted by Paalanne et al. [35] are simulated. This study used a computerized strain gauge dynamometer for the measurement of maximal isometric trunk muscle strength in standing position. Resting pads were placed against proximal part of pelvis and sternum with the purpose of stabilizing pelvis. With the intention of simulating the stabilized pelvis, the pelvis joint is fixed. Consequently, it cannot translate or rotate. Furthermore, with the aim of enhancing simulation time, nonessential joints are locked as well. This applies to the following joints: hip, knee, ankle, elbow and wrist. As a result, the number of DOF is brought down to 43. The 552 muscles and 20 point actuators are, contrarily, preserved throughout static analysis.

To compute maximal isometric extension in sagittal plane, the external load is applied to the 6^{th} and 7^{th} thoracic vertebrae (Fig. 2.3). In order to facilitate maximal isometric flexion force in sagittal plane, Schmid et al. [43] applied an external load to the sternum. It is worthy of note that Schmid et al. [43] modelled sternum as claviculae, scapulae and arms. Therefore, applying a force to sternum gives rise to the application of an external force at claviculae, scapulae and arms. Subsequently, muscles featuring attachment points to specified bodies get activated throughout analysis. Alternatively, as a means to quantify maximal isometric flexion in sagittal plane, external loads are applied to the 6^{th} and 7^{th} thoracic vertebrae (Fig. 2.3).

With the object of establishing maximal isometric strength, two external load files are fabricated. Designated external load files comprise incremental external forces of 10-N with a range of 0 – 700-N.

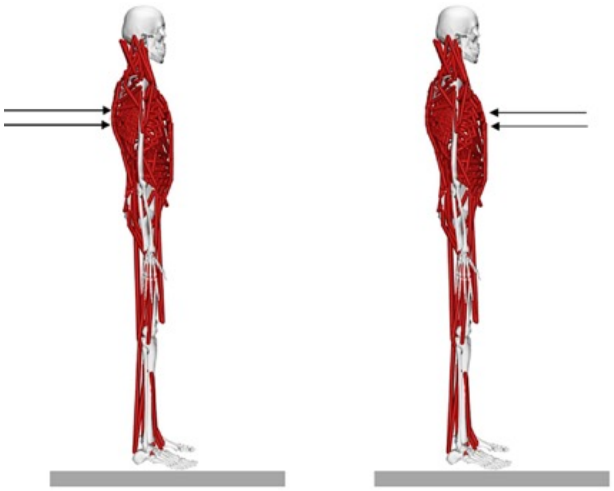

Figure 2.3: illustration of the applied external loads in sagittal plane. The *grey bars* represent the ground whereas *black arrows* represent the applied external loads. Assessment of maximal isometric extension is demonstrated on the left. Assessment of maximal isometric flexion is demonstrated on the right.

Figure 2.3 transpires external loads are applied to the 6^{th} and 7^{th} thoracic vertebrae to compute maximal isometric extension (left) and maximal isometric flexion (right). It should be emphasized that external loads applied to the 6^{th} and 7^{th} thoracic vertebrae are identical.

2.2.2. Maximal isometric force in frontal plane

For help in resolving maximal isometric force in frontal plane, the in vivo experiment conducted by Thomas et al. [49] is mimicked. In the study from Thomas et al. [49], participants were requested to stand in an upright position inside a restraint frame that stabilized the pelvis. Therefore, as a means to simulate the in vivo environment, the pelvis joint is locked. With reference to simulation time, nonessential joints, as indicated in section 2.2.1, are locked as well.

Thomas et al. [49] applied a lateral bend load in the form of a vertical force at the shoulder. Since the vertical force is distributed over the shoulder, the external load is applied to humerus, scapulae and claviculae (Fig. 2.4). The external load file comprises incremental external forces of 10-N with a range of 0 – 700-N.

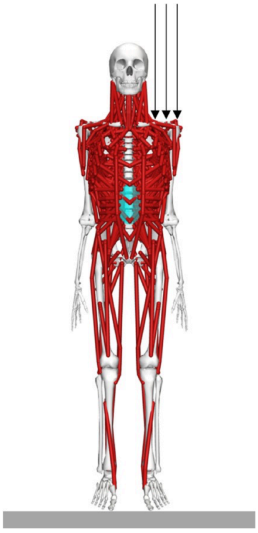

Figure 2.4: illustration of the applied external loads in frontal plane. The *grey bars* represent the ground whereas the *black arrows* represent the applied external loads. The external load is applied to humerus, scapulae and claviculae.

As illustrated in figure 2.4, three vertical external loads are applied to the left shoulder. Total external load is defined as the sum of the three vertical loads.

2.3. Static optimization outcomes

Once the *Static Optimization Tool* started to fail consistently, the model is considered too weak to resist the applied loads and therefore, maximal isometric force is characterized as the highest applied load for which the *Static Optimization Tool* successfully solved [46]. On top of that, maximal isometric force is determined with a precision of 8 decimals.

2.4. Summary

Chapter 2 covers the methodology considering the establishment of maximal isometric strength in sagittal and frontal plane. In total, three external load files are generated whereupon the external load is increased by an incremental force of 10-N. For assuring maximal isometric flexion and extension in sagittal plane, external loads are applied to the 6^{th} and 7^{th} thoracic vertebrae. To resolve maximal isometric strength in frontal plane, external loads are applied to the shoulder. So as to simulate in vivo circumstances, the pelvis joint is locked. Hip, knee, ankle, elbow and wrist joint are considered not important for static analysis. Indicated joints are, therefore, locked and as a consequence, the number of DOF is brought down to 43. On the condition that the *Static Optimization Tool* starts to fail consistently, maximal isometric force is obtained.

3

Dynamic analysis

This chapter deliberates the spinal stabilization system and the implementation of corresponding subsystems in the OpenSim model developed by Schmid et al. [43]. With the intention of simulating car-passenger interaction, vehicle perturbations, imitated by a translational perturbation signal in anterior-posterior direction, are discussed. To reduce computation time, structural constraints are introduced and muscle parameters are scrutinized, which will be further elaborated upon. To establish scientific evidence that the model is capable of delivering accurate outcomes, validation process is described.

3.1. Spinal stabilization system

The spinal stabilization system consists of three subsystems: the passive musculoskeletal subsystem, the active musculoskeletal subsystem and the neural and feedback subsystem. The passive musculoskeletal subsystem includes vertebrae, facet articulations, intervertebral discs, spinal ligaments and passive mechanical properties of the muscles [36]. The active musculoskeletal subsystem consists of muscles and tendons. Lastly, the neural and feedback subsystem consists of various force and motion transducers, located in muscles, tendons and neural control centers [36].

The function of the stabilizing system is to provide sufficient stability to the spine to match instantaneously varying stability demands due to changes in spinal posture, and static and dynamic loads [36]. The model developed model by Schmid et al. [43] includes bones, muscles and tendons and, therefore, incorporates the active musculoskeletal subsystem. However, the passive musculoskeletal subsystem and the neural and feedback subsystem are not included. Therefore, upcoming sections describe the implementation of components of the passive subsystem and components of the neural and feedback subsystem.

3.1.1. Passive subsystem

Intervertebral translations and rotations are likely dependent on intervertebral joint properties. Despite that, spinal ligaments and mechanical muscle properties are not included in the OpenSim model. Components of the passive subsystem do not provide any significant stability to the spine in the vicinity of the neutral position [36]. It is towards the ends of the ranges of motion that the ligaments develop reactive forces that resist spinal motion. The passive components probably function in the vicinity of the neural position as transducers for measuring vertebral positions and motions [36]. Hence, this subsystem is passive only in the sense that it by itself does not generate or produce spinal motions.

Mechanically, the amount of joint moves will depend both on the stiffness of the joint and the external loading applied to the joint [42]. This is believed to play a role in the amount of motion seen at each level of the spine [27]. Intervertebral joint properties have been measured in a variety of studies, using both coupled and uncoupled measurement approaches. In general, multibody musculoskeletal models continue to assume uncoupled motion, likely because of the lack of a general method to determine reasonable intervertebral translations [18]. The model from Schmid et al. [43] assumed uncoupled vertebral motions as well. On that account, uncoupled stiffness and damping parameters are considered

important. Markolf et al. [27] determined uncoupled stiffness and damping parameters from cadaveric studies. Indicated stiffness and damping parameters for each intervertebral joint is outlined in table 3.1.

Intervertebral joint	Stiffness (Nm/rad)	Damping (Nm/rad)
$\mathcal{L}1$ - $\mathcal{L}2$	100.0	7.5
$\mathcal{L}2$ - $\mathcal{L}3$	100.0	7.5
$\mathcal{L}3$ - $\mathcal{L}4$	100.0	7.5
$\mathcal{L}4$ - $\mathcal{L}5$	100.0	7.5
$\mathcal{L}5$ - $\mathcal{S}1$	100.0	7.5

Table 3.1: mean uncoupled stiffness and damping parameters at each intervertebral joint in sagittal plane. Parameters are obtained from cadaveric studies [27]. It is assumed intervertebral damping is identical for lumbar joints.

It is noteworthy to mention that limited data is available to characterize intervertebral damping. As a consequence, it is assumed intervertebral damping is identical for lumbar joints. That being the case, additional in vitro measurements would be beneficial. Effects of intervertebral joint properties on model kinematics are revealed in chapter 4.

Uncoupled stiffness and damping parameters are applied at joint centers as 6×6 matrices using expression-based bushings [30]. As mentioned previously, lumbar stabilization analysis is performed in sagittal plane. Therefore, translational stiffness and damping properties are neglected. Rotational stiffness and damping in sagittal plane are, on the other hand, incorporated in analysis. Subsequently, the bushing element in OpenSim encloses a single rotational spring-damper. Consequently, the uncoupled matrices have a single nonzero stiffness parameter. Equation 3.1 represents an uncoupled stiffness matrix

$$\begin{bmatrix} \mathrm{M}_x \\ \mathrm{M}_y \\ \mathrm{M}_z \\ \mathrm{F}_x \\ \mathrm{F}_y \\ \mathrm{F}_z \end{bmatrix} = \begin{bmatrix} 0 & 0 & 0 & 0 & 0 & 0 \\ 0 & 0 & 0 & 0 & 0 & 0 \\ 0 & 0 & \mathrm{k}_1 & 0 & 0 & 0 \\ 0 & 0 & 0 & 0 & 0 & 0 \\ 0 & 0 & 0 & 0 & 0 & 0 \\ 0 & 0 & 0 & 0 & 0 & 0. \end{bmatrix} \begin{bmatrix} \theta_x \\ \theta_y \\ \theta_z \\ \delta_x \\ \delta_y \\ \delta_z \end{bmatrix} \tag{3.1}$$

where M and F represent moments and forces produced by the bushing, θ and δ are rotations and translations of the joint, and k_1 represents the rotational stiffness parameter operating in sagittal plane [30]. The equation embracing damping rather than stiffness, is indistinguishable from equation 3.1.

The bushing element computes the force and moment proportional to the relative motions of two frames [6]. The approximate similarity between the bushing element and the intervertebral joint has led to its increased use in musculoskeletal models of the spine [6]. In general, the bushing element in OpenSim encloses three linear and three torsional spring-dampers, which act along or about the frames. Above-stated, rotational stiffness and damping operating in sagittal plane are exclusively incorporated in analysis. Bushing element computations are generated for the following motion segments: $\mathcal{L}1$ - $\mathcal{L}2$, $\mathcal{L}2$ - $\mathcal{L}3$, $\mathcal{L}3$ - $\mathcal{L}4$, $\mathcal{L}4$ - $\mathcal{L}5$ and $\mathcal{L}5$ - $\mathcal{S}1$. Summarily, five bushing force elements are implemented to simulate passive structures surrounding lumbar joints. Figure 3.1 exemplifies the bushing element computation for the $\mathcal{L}4$ - $\mathcal{L}5$ motion segment.

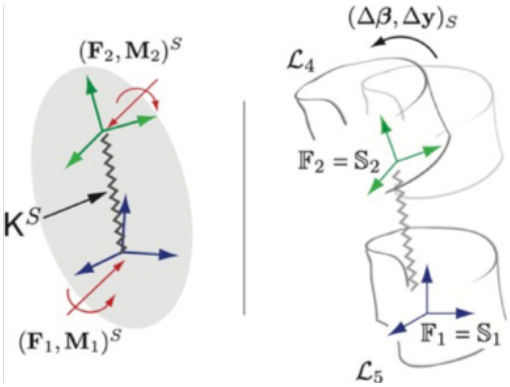

Figure 3.1: schematic of a bushing element computed for the $\mathcal{L}4$ - $\mathcal{L}5$ motion segment. By definition, the forces and moments exerted on the vertebral bodies due to the bushings are applied at the bushing frames for the $\mathcal{L}4$ - $\mathcal{L}5$ motion segment. Schematic retrieved from [6].

$\mathbb{S}1$ and $\mathbb{S}2$ symbolize frames which are situated at the origins of the vertebral bodies $F1$ and $F2$. The forces and moments due to bushing element are exerted at the origins of the $\mathbb{S}1$ and $\mathbb{S}2$ frames and are related to the increments in relative motion between the two frames ($\Delta\gamma$, $\Delta\beta$).

3.2. Neural and feedback subsystem

Neuromuscular control involves the subconscious integration of sensory information that is processed by the central nervous system, resulting in controlled movement through coordinated muscle activity [40]. The ability to stabilize our body while being perturbed requires accurate estimation about the orientation of the body with reference to gravity as well as the relative relationship between body segments [39]. Body segments are connected by mobile joints. Functional joint stability is achieved through the integration and complementary relationship between static and dynamic components of joint stability [45].

Visual, vestibular and somatosensory systems are the main sensory systems involved in postural control and balance [16]. Sensory feedback regulates the mechanical properties of the musculoskeletal system and is critical for proper sensory-motor control [3]. Proprioceptive feedback, on the contrary, entails the physical interactions with the environment that allow humans to build a sense of where their body begins and ends in space, even without vision [50]. This feedback is provided by specialized receptors in muscle that includes muscle spindles, Golgi tendon organs and joint feedback. Additionally, appointed feedback is key to maintaining dynamic and static muscle tone [50]. The sense of proprioception is ubiquitous and is essential for the coordination of the body [47]. In the study, features depicted in conceptual scheme 3.2, are considered in OpenSim.

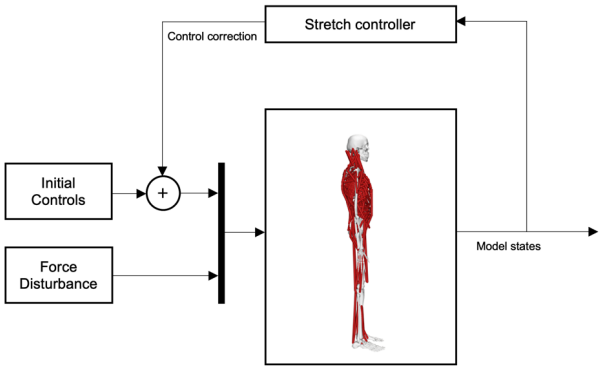

Figure 3.2: conceptual scheme of the human neuromuscular control system. Muscles convert neural activation signals into force. Thereafter, information concerning the state is sent back to the brain via a negative feedback mechanism.

Initial controls, as depicted in figure 3.2, propose muscle co-activation and are computed from the *Static Optimization Tool*. Initial controls are employed to maintain stability before control corrections are necessary. The stretch controller, incorporating proprioceptive feedback, computes control correction signals, thereby contributing to muscle activity [7]. Accordingly, despite disturbances, muscles maintain postural stability.

Perturbations mimicking car-passenger interaction are present and implemented to alter sensory feedback and their relationships with motor output. Importantly, perturbations can involve physical and sensory alterations and modify relationships within the balance control such that their effects are a function of the action of the subject [39]. Kinematics in response to perturbations caused by vehicle movements are studied.

In the present research, proprioceptive feedback is considered whereas visual and vestibular feedback mechanisms are disregarded. The proprioceptive feedback mechanism consists of musculoskeletal sensors of which muscle spindles and Golgi tendon organs are considered most important.

3.2.1. Stretch reflex

The stretch reflex, or more accurately myotatic reflex, is the most basic reflex pathway in the body and describes the muscle contraction in response to stretching within the muscle [5]. The stretch reflex is designed as a protective mechanism and functions to maintain the muscle at a constant length. When muscles lengthen, the muscle spindles are stretched. Muscle spindles have been found to play an important role in kinanesthesia and reflexive adjustment to perturbations [22]. This stretch activates muscle spindles which in turn send an impulse to the spinal cord. In terms of engineering principles, the stretch reflex arc is a negative feedback loop used to maintain muscle length at a desired value [44]. The appropriate muscle length is specified by the activity of descending pathways that influence the motor neuron pool [22]. This desired muscle length represents the desired CE length only as the muscle spindles sense active fiber length. Hence, tendon length (PE) is not included. It is essential to note, desired muscle length will vary with posture and task. When stretch is detected, the antagonistic muscles are inhibited and the agonist muscles contract. The stretch reflex is not controlled by the brain and is a monosynaptic response that is transmitted to the spinal cord [54]. Additionally, this reflex can be activated by external and internal forces.

The stretch reflex, implemented by means of a *Muscle Fiber Stretch Controller* [9], computes the instantaneous excitation, x_m, according to equation 3.2

$$x_m(t) = k_p(l_n(t) - l_d)_+ + k_v(\dot{l_n}(t))_+ \tag{3.2}$$

where k_p is the gain on normalized muscle stretch and k_v is the gain on normalized muscle stretch velocity. Normalized muscle stretch is computed as the difference between the current normalized muscle fiber length, l_n, and the desired normalized muscle fiber length, l_d. Both are normalized by the optimal muscle fiber length. Normalized muscle stretch velocity, $\dot{l_n}$, is computed as the ratio of current muscle fiber lengthening velocity to the maximum contractile velocity of the muscle. Furthermore, only positive muscle stretch and velocity are considered, as indicated by the parentheses, $()_+$, in equation 3.2. Since the stretch controller is a function of unitless muscle fiber states, parameters are unitless quantities.

To quantify effects of designated control parameters on lumbar stabilization, k_v, k_p and l_d are set to 0.0 0.1, 0.5 and 1.0. Bearing in mind that these simulations serve to exemplify contribution of extrinsic properties, reflexive control parameters are equal for all muscles. On condition car-passenger interaction is simulated, muscles are grouped. Muscles in a group share identical k_v and k_p. Contrarily, l_d is equal to 1.0 for all muscles. In such manner, muscles respond to stretch as soon as muscles surpass optimal muscle fiber length. Thereafter, reflexive control parameters are estimated by way of an optimization scheme. Associated results are debated in upcoming chapter.

3.2.2. Muscular control parameter estimation

As described in section 3.1.1, intervertebral stiffness and damping parameters are assembled from literature. Oppositely, reflexive control parameters are resolved by means of an optimization. It is equivocal to assume all muscles possess equal stretch parameters. Moreover, selecting identical reflexive control parameters for all muscles entailed mediocre results. Therefore, for final analysis, muscles are grouped based on their function. In conclusion, nine muscle groups are established in which muscles share identical reflexive control parameters. Equivalent procedure is followed by Demers et al. [9].

By virtue of Gauss-Newton optimization, a common optimization scheme for solving unconstrained non-linear least squares problems, optimal k_v and k_p values are selected [19]. Gauss-Newton optimization minimizes the error between simulated kinematics and experimentally measured kinematics. The advantage of the Gauss-Newton method is that it requires only first order information. Additionally, it is known to be able to achieve local quadratic convergency rate [11]. The method iteratively updates the computed solution with a step toward minimizing the objective function. In the present study, the objective function defines the error between simulated kinematics and experimentally measured kinematics throughout the duration of the simulation. The optimization uses the reflexive control parameters as design variables. Consequently, the algorithm selects k_v and k_p that minimizes the objective function.

To identify effects of reflexive control, optimization scheme is utilized under two scenarios. First scenario corresponds to lumbar settling in absence of force disturbance. Under this scenario, the error between model kinematics and a reference signal corresponding to zero rotation, is minimized. Second scenario involves car-passenger interaction in which the error between model kinematics and experimentally measured kinematics is minimized.

For a linear model, convergence for Gauss-Newton method will be rapid and not depend heavily on initial parameter estimates. Be that as it may, as the magnitude of model non-linearity becomes more prominent, convergence will be slow and resulting parameters may not be reliable. Taking into consideration that improper initial values can lead to local, but not global, minimum of the residual sum of squares, proper initials are essential. By means of manual tuning, appropriate initial values are established.

3.2.3. Postural activity

Postural tone, often associated with anti-gravity support, is centrally important in the control of standing posture [28]. Anti-gravity support is partly provided by passive bone-on-bone forces in joints, stretched ligaments and muscles. However, it additionally requires active muscle activations [3]. Increased muscle co-activation is thought to be an important part of the adaptation process in that it helps to reduce movement errors [3]. Muscle co-activation occurs when agonist and antagonist muscles, surrounding a joint, contract simultaneously [14]. Individuals are able to modulate stiffness by co-activating muscles in anticipation of movement. As muscles contract simultaneously, which produces compression on the joint, the joint is able to become stiffer and provide equilibrium [55]. Co-activation does, however, not always provide stability. This is attributable to the shape of force-length characteristic. On the occasion muscles exceed optimal fiber length, slope of force-length curve is negative. Inevitably, muscles are destabilising.

Co-activation can be measured using EMG from the contractions that occur [23]. In spite of that, the general mechanism is still widely unknown. Initially, the model developed by Schmid et al. [43] did not include any information on muscular antagonism. Therefore, many muscles do not have the activity that they are supposed to have. That being the case, controllers activating specified muscles at a prescribed constant value throughout simulation, are added. It is recalled that center of gravity (COG) is modelled 9.1-cm anterior to $\mathcal{L}4$. As a consequence, in the circumstance abdominal and spinal muscles possess equal prescribed constants, it shall be so that trunk flexes. Accordingly, spinal muscles surrounding lumbar joints (i.e. sacrospinalis and transversospinalis) show strongest contributions on muscular level for maintaining postural control. Human beings do, however, not remain fixed in anatomical position. As a matter of course, COG changes constantly with new position of body and limbs.

Co-activation can be defined as any activation of muscles that generate no net torque. For a multi-muscle multi-joint system, as the model from Schmid et al. [10], there are infinite muscle co-activation patterns that the central nervous system can select. How the central nervous system selects one of these infinite muscle patterns is still an open question. To establish muscle co-activation patterns, the *Static Optimization Tool* is evoked. The model is constrained to static posture and throughout analysis, $\mathcal{L}1 - \mathcal{L}2$, $\mathcal{L}2 - \mathcal{L}3$, $\mathcal{L}3 - \mathcal{L}4$, $\mathcal{L}4 - \mathcal{L}5$, $\mathcal{L}5 - \mathcal{S}1$ and pelvis are free to move in sagittal plane. Muscle co-activation, under the effect of gravity, is recorded. As declared in paragraph 2.3, the *Static Optimization Tool* minimizes the sum of squared muscle activation. Attributable to the fact that minimum effort solutions tend to underestimate muscle co-activation [7], absolute static posture could not be achieved.

Altered postural control is predominantly associated with increased muscle co-activation [3]. With the object of achieving static posture, the level of muscle co-activation is varied and mechanical joint impedance is altered. Increases in muscle co-activation is interpreted as a strategy to provide additional postural stability. This is accomplished by increasing minimal muscle activation level. By default, minimal and maximal muscle activation are set to 0.010 and 1.0, respectively. To quantify effects of increased muscle co-activation, minimal muscle activation level is set to 0.011, 0.020 and 0.070. Subsequently, the *Static Optimization Tool* is, once more, evoked to yet acquire static posture.

3.3. Forward dynamics

For the purpose of running a forward dynamics simulation, an iterative method is used to advance the model dynamics over specified time intervals [29]. Model outputs comprise time histories of all calculated variables. Muscle-actuated forward dynamics simulations are particularly powerful due to the fact that they allow for the identification of causal relationships between the neural control inputs, muscle force and power output, and task performance [34]. Forward dynamics calculates motion (q, $\dot{q}$, $\ddot{q}$) from force τ by virtue of integrating specified initial conditions [29].

OpenSim incorporates forward dynamics by the *Forward Dynamics Tool* [8][46]. The OpenSim *Forward Dynamics Tool* uses a neural demand from an input controls file to generate an output states file. By making use of musculotendon dynamics, forces actuating the model are computed. Thereupon, joint moments, by means of musculoskeletal geometry, are determined. By way of multibody dynamics, accelerations and other state derivatives are calculated and ultimately, state derivatives are numerically integrated to determine the model's new states [25]. Once a model is evaluated, typically by assessing how closely it can reproduce the recorded performances of an individual, it can be applied to investigate cause and effect relationships. Assumptions and constraints necessary to model the human body must be critically reviewed in relation to the true human dynamical system.

3.3.1. Computation time

As aforementioned, Schmid et al. [43] predicted and validated trunk muscle strength. This alludes dynamic response is yet to be determined. In early stages, it came to light that Schmid et al. [43] rotated the model with respect to z-axis. That being the case, gravity operated in z and y-direction. To combat implied phenomenon, pelvic frame and ground frame are aligned at neutral. Hence, the model has zero pelvic tilt with respect to ground. Furthermore, it is learned that Schmid et al. [43] developed an exceptionally stiff model. Since integrator has to take many small steps, forward dynamics simulations are demanding.

The contribution of inertia is an inherent and crucial feature of dynamic systems [51]. Low inertia can negatively affect the system. Therefore, with the object of foreshorten computation time, model inertia is scrutinized. Thenceforth, normalized fiber length is investigated. As reported in figure 3.3, in event of muscles being stretched out to 2 or more times their optimal fiber lengths, passive force-length curve becomes practically vertical. It follows that computation time rises and large result files are generated.

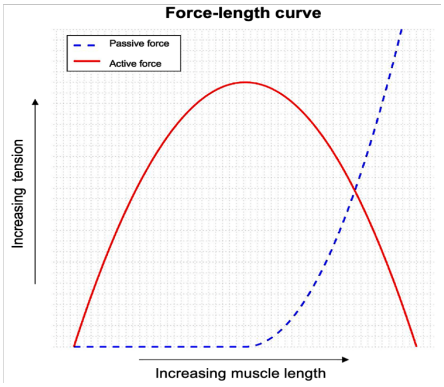

Figure 3.3: force-length relationship. Indicated relationship describes dependence of the steady-state isometric force of muscles as a function of muscle lengths. Passive muscle force (*dotted line*) arises from elastic spring-like elements stretched beyond their resting length. By contrast, active muscle force (*solid line*) is generated by processes within the sarcomere.

Tendon slack length is sensitive to the operating region on the force-length curve [1]. Despite the fact that cadaver studies report optimal fiber length, tendon slack length is infrequently reported [20]. In light of this, small adjustments are justified. Therefore, on condition muscles act at suboptimal fiber lengths, tendon slack length is modified. The subsequent muscle behaviour is sensitive to parameter changes and as a result, tendon slack length has significant effects on model kinematics. Designed to meet the need of abbreviating computation time, muscle parameter changes are made. With the intention of tracking computation time, number of integrator steps is assessed.

As declared in paragraph 2.1, throughout static analysis, 552 muscles are embedded in the model from Schmid et al. [10]. Taking into account the fact that throughout dynamic analysis focus is on lumbar stabilization, inconsequential muscles are removed from the model. Hence, following muscle groups are omitted from the model: neck, peroneus, gastrocnemius, trapezius and serratus anterior. Accordingly, throughout dynamic analysis, the model comprises 274 muscles. Appendix B encapsulates overview of embedded muscles throughout dynamic analysis.

3.3.2. Structural constraints

As a rule of thumb, forward dynamics simulation models have remained as simple as possible while maintaining sufficient complexity to answer the research question [29]. It is often claimed that the simpler the model, the easier it is to quantify the contributions of its features to the observed effect. However, in reality, model complexity is more often limited by computation power and the ability to construct scientifically robust constraints [29].

In light of the fact that abdominal muscles are wrapped over the peritoneum, Schmid et al. [43] implemented an ellipsoid for abdominal muscle wrapping. Additionally, Schmid et al. [43] connected sacrum and abdominal wrapping surface by means of a revolute joint. Considering the fact sacrum does not move with respect to z-axis, the abdominal wrapping surface remains stationary in the event of lumbar bending, thereby giving rise to unreliable abdominal motion. By selecting $\mathcal{L}5$ as parent frame, in place of sacrum, abdominal wrapping surface moves with respect to z-axis in the course of lumbar bending.

Spinal joints modelled by Schmid et al. [43] incorporate 3-DOF. Inasmuch as center of attention is on lumbar stabilization in sagittal plane, spinal joints are converted to revolute joints. As a result, lumbar joints can exclusively move in sagittal plane. In the event of simulating car-passenger interaction, pelvis joint is free to move in anterior-posterior direction. Remaining joints are, on the contrary, locked, thereby enhancing computation time. That being the case, the simplified model retains 6-DOF being translational pelvis motion which is externally prescribed, and flexion at the 5 lumbar joints being $\mathcal{L}1 - \mathcal{L}2$, $\mathcal{L}2 - \mathcal{L}3$, $\mathcal{L}3 - \mathcal{L}4$, $\mathcal{L}4 - \mathcal{L}5$ and $\mathcal{L}5 - \mathcal{S}1$.

3.4. Vehicle perturbations

Neural alterations, feedback mechanisms and the forward dynamics simulation process are clarified in previous sections. On that account, upcoming sections focus on the simulation of vehicle perturbations. With the intention of simulating car-passenger interaction, literature is consulted.

3.4.1. Platform translations

Van Drunen et al. [10] identified motor control in low-back stabilization by simultaneously quantifying intrinsic and extrinsic contributions. During experiments, subjects assumed a kneeling-seated posture, while being restrained at the pelvis. A translational platform perturbation is applied in anterior-posterior direction and as a consequence, upper body sway is evoked.

Perturbations were random-appearing multisine signals of 20-s duration. Fade-in and fade-out periods were applied to minimize transient behaviour and to prevent abrupt platform motions. Van Drunen et al. [10] employed perturbation signals incorporating 0.2-Hz as lowest and 1, 3 and 10-Hz as highest frequency. High bandwidth perturbations do not fully represent intrinsic and extrinsic behaviour during most daily life activities [10]. Accordingly, in the present study perturbation with lowest bandwidth is employed for further analysis. On this wise, perturbation signal contains 0.2-Hz as lowest frequency and 1-Hz as highest frequency. Unfiltered perturbation signal, attained from Van Drunen et al. [10], is illustrated in figure 3.4.

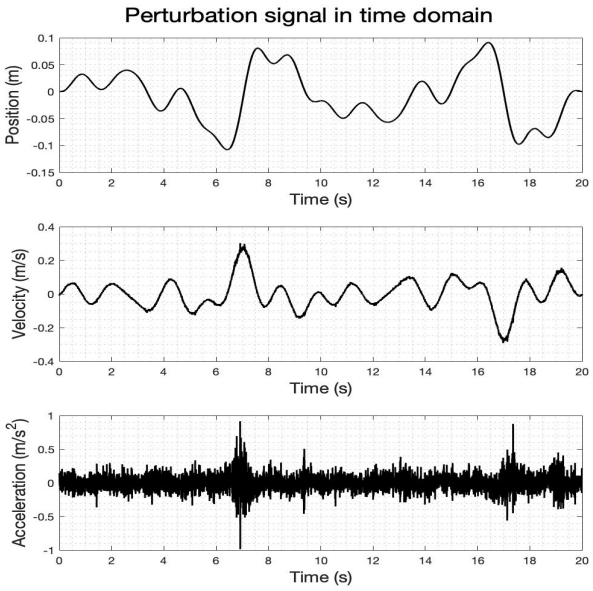

Figure 3.4: unfiltered perturbation signal attained from Van Drunen et al. [10] as time series. Perturbation signal is shown as position (*top*), velocity (*middle*), and acceleration (*bottom*) signal. Illustrated signal is a random-appearing multisines of 20-s duration.

As demonstrated in figure 3.4, platform perturbation signal incorporates noise, especially at higher frequencies. Underlying trend is determined with the aid of a low pass filter with a passband frequency of 2-Hz. Consequently, frequencies below 2-Hz are allowed whereas frequencies above 2-Hz are attenuated [2]. Perturbation signal after employing a low pass filter, is presented in figure 3.5.

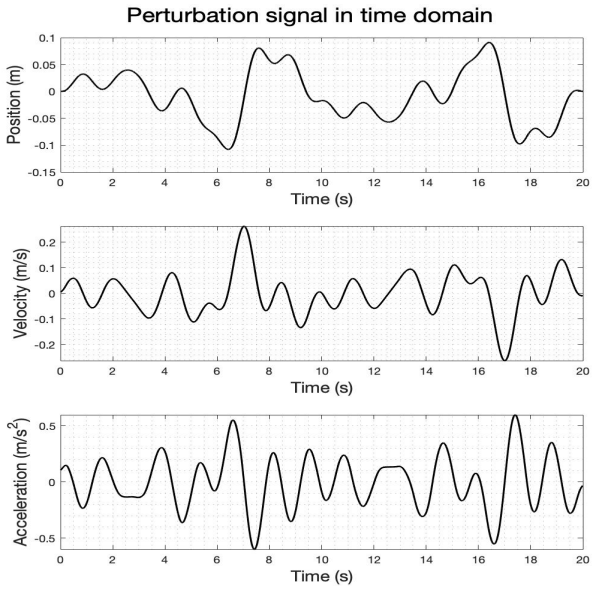

Figure 3.5: filtered perturbation signals as time series. Perturbation signal is shown as position (top), velocity (middle), and acceleration (bottom) signal. Illustrated signal is a random-appearing multisines of 20-s duration.

Figure 3.5 encapsulates that on the strength of filtering, noise ceases to be visible. This indicates that platform translations, simulating vehicle perturbations, could be applied to the OpenSim model.

3.4.2. Perturbation employment

Van Drunen et al. [10] benefitted from platform accelerations and did, therefore, not apply pelvis perturbations directly on the effective trunk mass. Conversely, in the present study, external forces are applied directly to the pelvis. To limit impact of pelvis perturbations on remaining body parts, pelvis mass is increased to 10.000-kg. It is, however, noteworthy to mention that the *Forward Dynamics Tool* demands a force perturbation. Therefore, by multiplying platform accelerations with the fictitious pelvis mass of 10.000-kg, the exerted force is identified. A .mot (motion) file accommodating external loads is constructed and through the medium of an XML file, the force disturbance is appended to the OpenSim model. Intending to prevent abrupt translational motion, a fade-in period of 2-s is adapted.

3.5. Forward dynamics simulation outcomes

As indicated previously, Van Drunen et al. [10] evoked body sway in anterior-posterior direction and incorporated trials in which subjects had to keep their eyes closed. Visual feedback was, thereby, ruled out. Since visual feedback is not included in the musculoskeletal model, associated trials are used for validation purpose. In the research from Van Drunen et al. [10], local segmental rotations were based upon experimental markers at vertebral bodies. Acquired experimental data comprises lumbar kinematics of six participants. Trials are repeated twice and each trial encompasses three repetitions. Signal averaging, a signal processing technique applied in time domain, is considered. Firstly, kinematics are averaged across repetitions and trials and secondly, kinematics are averaged over subjects.

In short, in the present study, lumbar rotation is assessed in sagittal plane. Lumbar rotation is based on the angle of the link between $\mathcal{S}1$ and $\mathcal{L}1$ with the vertical axis. Thereafter, model rotations are compared with experimental translations found by Van Drunen et al. [10]. To quantify optimal control parameters, Gauss-Newton algorithm is employed. The objective function, defining the error between simulated kinematics and measured kinematics, is minimized. Despite the fact that reflexes are involuntary, humans are capable of altering reflexive settings [10]. In an effort to explore the indicated, optimization scheme is utilized under two scenarios. First scenario corresponds to trunk settling whereas second scenario corresponds to car-passenger interaction.

With the aim of measuring discrepancy between the model and actual data, datasets should possess equal length. The length of model data and experimental data is, however, incompatible. In an effort to match specified length, model data is interpolated. Be that as it may, inasmuch OpenSim makes use of a variable time-step integrator, the iterated dataset is non-uniformly sampled. Experimental data is, on the contrary, sampled at a fixed rate. As sampling methods are opposed, model distribution and experimental distribution are dissent. It is, therefore, arduous to resolve model accuracy. In order to rectify the indicated, model kinematics and experimental kinematics are plotted against adequate time arrays. Following that, both curves are fitted by means of a shape-preserving-interpolant. In the resulting fit, each pair of consecutive points is connected by a different cubic polynomial.

The validity of the optimized model is assessed in time domain using the variance accounted for (VAF). The experimental lumbar kinematics of $\theta(t)$ are compared with the estimated model outcomes of $\theta_{mdl}(t)$:

$$VAF = 1 - \frac{\sum(\theta(t) - \theta_{mdl}(t))^2}{\sum(\theta(t))^2} \tag{3.3}$$

VAF measures the proportion to which the OpenSim model accounts for the variation of the experimental data set. A VAF of 1 reflects a perfect description of the measured signal by the model.

Finally, with the aid of system identification techniques, the frequency response function (FRF) is estimated to describe the kinematic response to perturbations. FRFs describe dynamic behaviour of a system as a function of frequency, where gain indicates magnitude of the output relative to the input, and FRF phase indicates the relative timing of the output relative to the input [10]. Kinematic FRF is derived as the open-loop response to the perturbation ($P(t)$) of the lumbar rotation in sagittal plane ($\theta_{mdl}(t)$)

$$\theta(f) = \frac{S_{P\theta}(f)}{S_{PP}(f)} \tag{3.4}$$

with $S_{P\theta}(f)$ representing estimated cross-spectral density between Fourier-transformed signals P and θ. The cross-spectral densities are only evaluated at frequencies containing power in the perturbation signal. So as to achieve noise reduction, cross-spectral densities are averaged across the six time segments and over two adjacent frequency points [10].

3.6. Summary

Chapter 3 discusses the methodology considering simulation of car-passenger interaction. Model alterations suchlike passive structures, co-activation and length-velocity feedback are debated. On account of similarity between a bushing element and intervertebral joint properties, passive structures surrounding lumbar joints are implemented by virtue of a *Bushing Force*. Muscular antagonism is not included in the model developed by Schmid et al. [43]. Consequently, many muscles do not have the activity that they are supposed to have. Muscle co-activation, determined from the *Static Optimization Tool*, gives rise to feedforward activation. Inevitably, muscles are activated at a prescribed constant value throughout analysis. Length-velocity feedback, playing an important role in kinanesthesia and reflexive adjustment to perturbations, is implemented by means of a *Muscle Fiber Stretch Controller* [9]. Furthermore, it is revealed that simulations converged towards small integrator steps resulting in outrageous computation time. Aiming to foreshorten computation time, inertial parameters and muscle properties are scrutinized.

For the purpose of simulating vehicle perturbations, platform acceleration exploited by Van Drunen et al. [10] is employed in forward dynamics simulation. Nevertheless, OpenSim demands a force perturbation. For that reason, platform acceleration is multiplied with the fictitious pelvis mass 10.000-kg. Accordingly, the exerted force is identified. In the fullness of time, lumbar kinematics established by Van Drunen et al. [10] are used for validation purpose.

4

Results

Validation of model estimates is critical to gain confidence in modelling results. This chapter starts with the assessment of static analysis in which an overview of muscles reaching their upper bound in the process of static optimization, is given. Thereafter, model predictions in sagittal and frontal plane are compared with in vivo measurements. After static analysis, dynamic analysis is assessed whereupon impact of neural alterations and feedback mechanisms are discussed. Ultimately, model kinematics are compared with findings obtained by Van Drunen et al. [10].

4.1. Static analysis: muscle activation

This paragraph gives an overview of muscles reaching their upper bound during the static optimization process. At the very time muscles reach their upper bound, muscles are considered too weak and the *Static Optimization Tool* fails. A visual representation of muscles reaching maximal activation is given in figure 4.1. It is remarkable that figure 4.1 consists of three separate illustrations. Figure on the left and in the middle represent muscle activation in the course of maximal isometric extension and flexion, respectively. Figure on the right shows muscle activation in time of maximal isometric flexion in frontal plane.

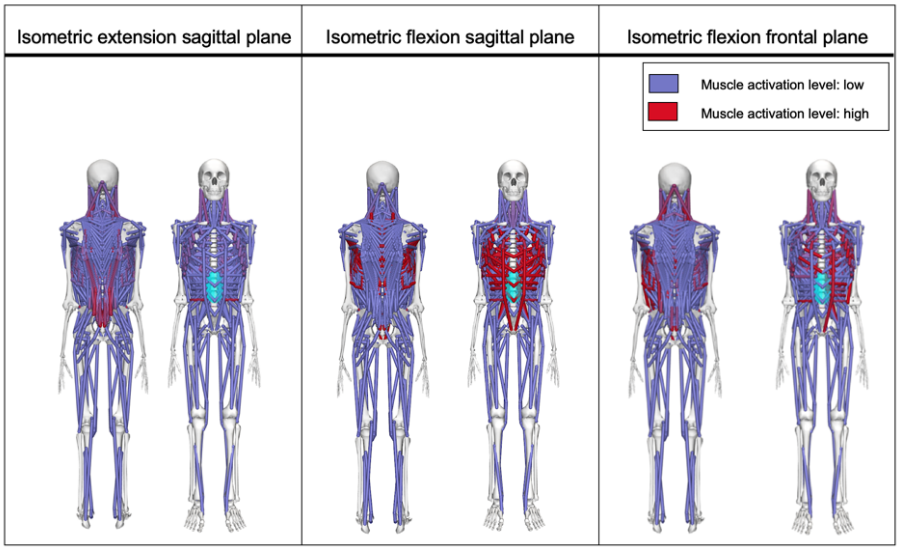

Figure 4.1: a visual representation of muscles reaching their upper bound in the course of maximal flexion and extension in sagittal and frontal plane. Figure on the left and in the middle represent muscle activation in the course of maximal isometric extension and flexion, respectively. Figure on the right illustrates muscle activation in time of maximal isometric flexion in frontal plane. Muscles coloring red represent elevated muscle activation level whereas muscles coloring purple represent low activation level.

Figure 4.1 illustrates that throughout isometric flexion analysis, internal oblique, external oblique, transversus abdominis and rectus abdominis show elevated activation levels. Contrariwise, in the course of isometric extension analysis, solely muscles in lumbar region (i.e. sacrospinalis and transversospinalis) exhibit raised activation levels. Difference in activation levels between isometric analysis is justified by the localization of the external force. A table revealing what exact muscles, as illustrated in figure 4.1, reach their upper bound, is included in Appendix A.

For the determination of isometric strength in sagittal plane, external forces are applied anteriorly and posteriorly. This allows for symmetric activation patterns. For the assessment of isometric flexion in frontal plane, an external force is employed in lateral direction. From that fact, an asymmetric activation pattern is revealed.

In short, from figure 4.1 it can be learned that in the event of isometric extension in sagittal plane, lumbar muscles reach their upper bound first. In case of isometric flexion in frontal plane, muscles on the left side of the model, reach their upper bound first. As the situation in isometric flexion in sagittal plane, abdominal muscles reach their upper bound first.

4.2. Static analysis: validation

Maximal isometric flexion and extension in sagittal plane predicted by the model are validated against outcomes identified by Paalanne et al. [35]. Maximal isometric lateral bending is, on the contrary, validated against outcomes retrieved from Thomas et al. [49]. An illustration involving model predictions and in vivo outcomes is generated in MATLAB 2021a (Fig. 4.2). Additionally, values found by Schmid et al. [43] are mentioned.

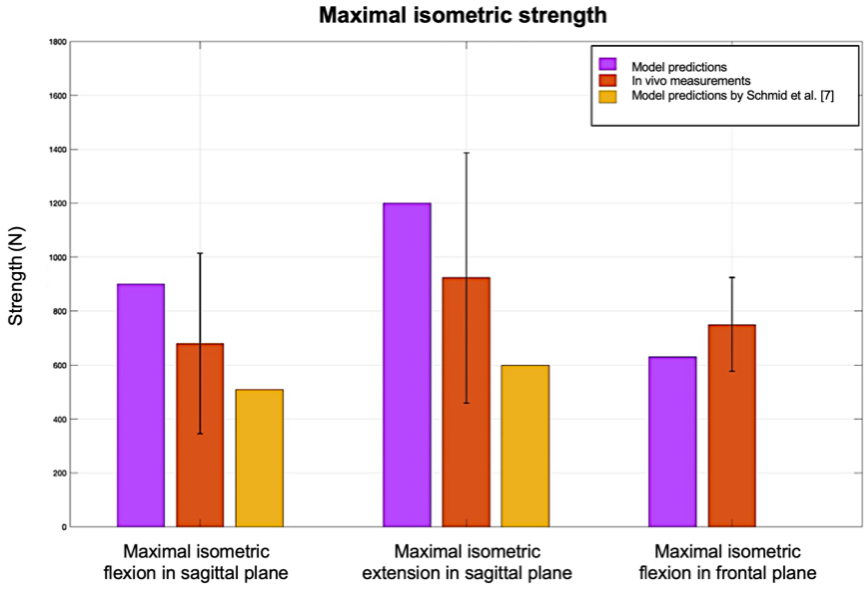

Figure 4.2: model predictions of maximal isometric force in sagittal and frontal plane in comparison with in vivo measurements conducted by Paalanne et al. [35] and Thomas et al. [49]. Purple bars indicate model predictions determined in present study, yellow bars indicate model predictions found by Schmid et al. [43] and orange bars indicate in vivo measurements. The error bars indicate the range found in literature.

Figure 4.2 shows model predictions and in vivo outcomes. It is discovered, model predictions lie within the range found by Paalanne et al. [35] and Thomas et al. [49]. As indicated earlier, maximal isometric force of numerous muscles is increased. It is, therefore, only expected that model predictions found in present study are superior to model predictions found by Schmid et al. [43]. The model predicted excessive extension strength in sagittal plane. Lowest model predictions are, on the contrary, found in the event of isometric flexion in frontal plane. Other than that, highest in vivo outcomes are found for isometric extension in sagittal plane and lowest in vivo outcomes are found for isometric flexion

in sagittal plane. It should be noted, as depicted by the error bars, a substantial range in isometric strength is found in literature.

4.3. Dynamic analysis: computation time

Initial simulations converged towards small integrator steps leading to excessive CPU taking 4.5-h to simulate 4-s. Increasing model inertia of $\mathcal{L}4$ and $\mathcal{L}5$ reduced the number of integrator steps with a factor 2.5. CPU, associated with number of integration steps, improved by a factor of merely 2.1. Apart from that, reducing spinal DOF, as hereinbefore described, brought the number of integrator steps down by a factor of 1.4. Thus, at this stage it takes 2.1-h to simulate 4-s. Accordingly, computation time remains a burden. To identify the issue, muscle properties are explored. Through the use of the *Analysis Tool*, normalized fiber length is investigated. Thenceforth, normalized fiber velocity is considered. It is revealed that muscles retain unreasonable muscle fiber velocity. By way of illustration, normalized fiber velocity of iliocostalis is exhibited in figure 4.3. It is worth bearing in mind, intrinsic properties are incorporated whereas extrinsic properties are omitted throughout muscle analysis.

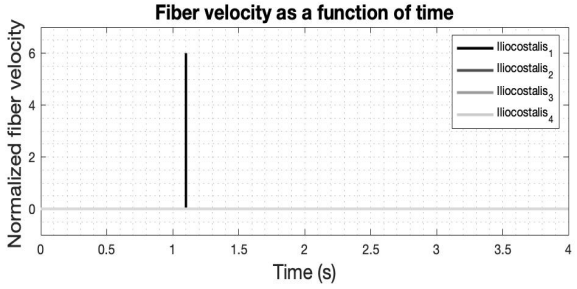

Figure 4.3: normalized fiber velocity of iliocostalis. Shortest muscle commences substantial fiber velocity and as a consequence, muscle starts to oscillate.

As appears from figure 4.3, peculiar behaviour can be observed. Figure 4.4 shows that by expanding tendon slack length of vibrating muscles, fiber velocity is abbreviated.

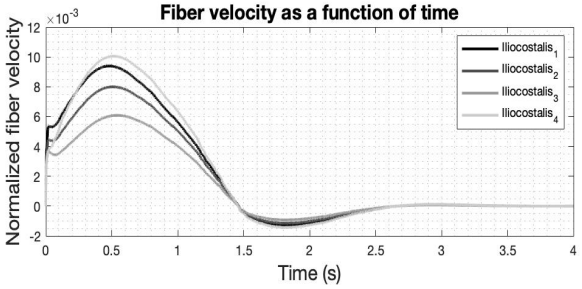

Figure 4.4: normalized fiber velocity of iliocostalis ensuing expanding tendon slack length. By way of expanding tendon slack length, normalized fiber velocity descends and large velocity spikes vanish.

It should be emphasized that expanding tendon slack length of iliocostalis does not imply the problem in consideration of computation time is dissolved.

For the purpose of addressing indicated behaviour, muscles are removed from the model. Thereafter, muscle groups are added to the model one by one. On the occasion a muscle group is added, forward dynamics simulation of 1-s is carried out and normalized fiber velocity is explored. Additionally, the number of integrator steps is considered. In absence of muscles, the number of integrator steps is equivalent to 16. Adding muscle groups to the model gives rise to an increased number of integrator steps. Hence, increased CPU. By amending tendon slack length, computation time is reinforced. Table 4.1 outlines progress regarding computation time. Exact adjustments with regard to tendon slack length are encapsulated in Appendix B.

Added muscle group	Number of muscles	Old integrator steps	New integrator steps
Sacrospinalis	76	322	43
Transversospinalis	74	640	77
Latissimus dorsi	28	1311	107
Quadratus laborum	36	1367	141
Internal oblique	12	1458	156
Extrernal oblique	14	1547	218
Transversus abdominis	10	1670	245
Rectus abdominis	2	2021	299
Psoas major	22	2548	318

Table 4.1: muscle groups are appended to the model one by one. At the occasion muscle group is added, number of integrator steps is explored. Afterwards, tendon slack length of oscillating muscles is modified and computation time is reinforced.

Table 4.1 discloses the amount of integrator steps with respect to appended muscle groups. Essential muscle groups are added to the model and in due course the number of integrator steps reduced from 2548 to 318. Ultimately, a simulation of 4-s took 30-s to solve.

4.4. Dynamic analysis: intrinsic properties

With the intention of illustrating effects of intervertebral stiffness and damping parameters, simulations for numerous stiffness and damping values are generated. Thereupon, effect of co-activation on modelling results are elucidated.

4.4.1. Impact passive joint properties

With the aim of illustrating impact of intervertebral joint properties, simulations for various stiffness and damping values are conducted. Implied simulations show lumbar stabilization in presence of gravity yet in absence of force disturbance. Moreover, throughout analysis, reflexive feedback and postural activity are omitted. Each contour in figure 4.5 represents rotation of the $\mathcal{L}5 - \mathcal{S}1$ joint in sagittal plane during a single simulation. To preserve computation time, remaining joints are locked throughout analysis. Stiffness and damping values are varied from 100 – 800-Nm/rad and 0 – 8-Nm/rad, respectively. Upper figure demonstrates variation of intervertebral stiffness whereas lower figure demonstrates variation of intervertebral damping. It is critical to state that positive rotation is associated with lumbar flexion. Conversely, negative rotation is associated with lumbar extension.

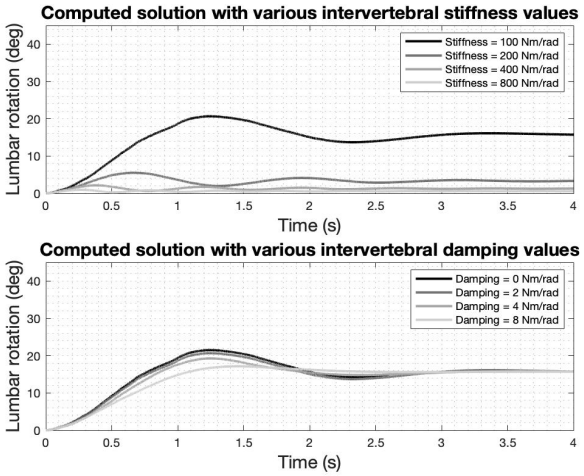

Figure 4.5: impact of several intervertebral stiffness and damping values on the rotation of $\mathcal{L}5 - \mathcal{S}1$ in sagittal plane. *Top* figure illustrates variation of intervertebral stiffness. Throughout indicated simulations, damping is retained constant at 0-Nm/rad. *Bottom* figure depicts variation of intervertebral damping in which case stiffness is kept constant at 100-Nm/rad.

Figure 4.5 demonstrates higher intervertebral stiffness initiate decreased lumbar flexion. Furthermore, amplitude decreases in the act of increased intervertebral damping. Ultimately, intervertebral properties exhibited in table 3.1 are adopted for further analysis. Therefore, intervertebral stiffness and damping values are set to 100 and 7.5-Nm/rad, respectively.

4.4.2. Impact postural activity

Co-activation is modelled as constant, feedforward activation of opposing muscle groups. With planned co-activation of abdominal and spinal muscles, a force is generated to stiffen the spine. Controls that constitute for postural activity are generated by the *Static Optimization Tool*. As stated in section 3.2.3, postural control is associated with increased muscle co-activation. Therefore, aimed at providing supplemental postural stability, muscle co-activation level is varied. To quantify effects, minimal muscle activation level is set to 0.011, 0.020 and 0.070. Impact of postural activity and subsidiary co-activation on lumbar rotation in sagittal plane, are exemplified in figure 4.6.

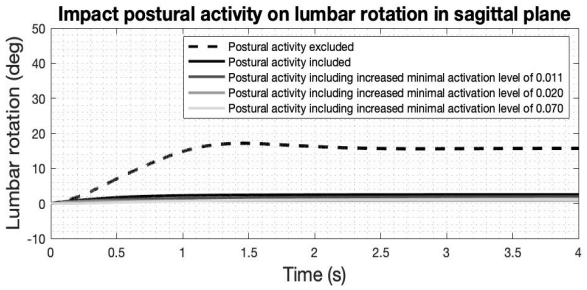

Figure 4.6: impact of co-activation on the rotation of $\mathcal{L}5$ - $\mathcal{S}1$ in sagittal plane. Altered postural control is associated with increased muscle co-activation. Level of muscle co-activation is increased and mechanical impedance is altered.

Ascribable to postural activity, lumbar flexion abates. It is, however, pertinent to note that in spite of postural activity, a lumbar flexion angle of 2-deg is perceptible. As per the fact that intensified muscle co-activation induces joint stiffness, lumbar flexion continues to abate. It is noteworthy to mention, minimal muscle activation levels of 0.020 and 0.070 generate equivalent lumbar kinematics. Finally, predicated on outcomes illustrated in figure 4.6, prescribed controls appertaining to a minimal muscle activation level of 0.020, are retained for further analysis.

4.5. Dynamic analysis: extrinsic properties

Intrinsic properties alone cannot be relied upon to generate enough torque to compensate for acceleration effects. Ongoing paragraph investigates contribution of extrinsic properties, such as length-velocity feedback on lumbar rotation in sagittal plane. Bearing in mind that these simulations serve to exemplify contribution of extrinsic properties, reflexive control parameters are equal for all muscles. Inasmuch as focus is on extrinsic properties, muscle co-activation is disregarded. In the interim, intervertebral joint stiffness and damping parameters carry on being 100 and 7.5-Nm/rad, respectively.

4.5.1. Impact length-velocity feedback

To quantify effects of k_v on lumbar stabilization, four simulations, varying gain k_v, are generated. k_v is set to 0.0, 0.1, 0.5, and 1.0. In the course of simulations, k_p and l_d remain invariable. Impact of k_v on lumbar kinematics is exemplified in figure 4.7. In view of the fact that k_v determines contribution of restoring force proportional to velocity, muscle stretch velocity as a function of time, is illustrated.

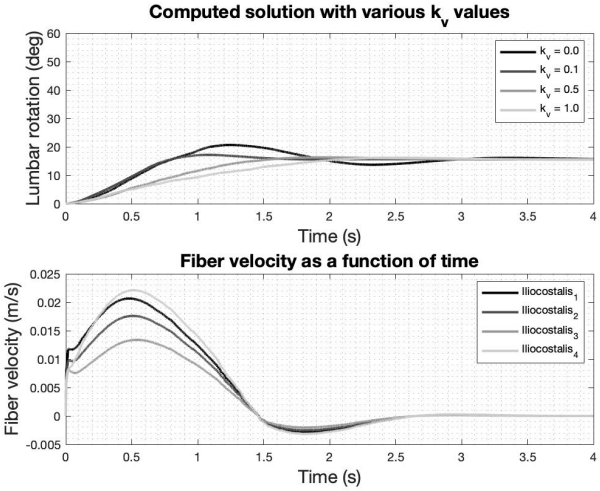

Figure 4.7: *top* figure exemplifies rotation of $\mathcal{L}5 - \mathcal{S}1$ joint in sagittal plane with various k_v values. Reflexes are modeled as feedback from the muscle lengthening speed to muscle excitations, with reflex intensity modulated using k_v. Each contour represents lumbar rotation in which muscles generate force with a constant reflex gain. k_v is varied from 0.0 to 1.0. *Bottom* figure exemplifies muscle stretch velocity as a function of time.

From figure 4.7 it is shown that k_v possesses potential for damping purpose. Endpoint rotation is not affected by k_v which is commensurate with logic seeing that fiber velocity approaches zero. Accordingly, k_v does not exert impact on lumbar kinematics. It deserves to be mentioned, positive velocity of muscle fibers indicates concentric contraction whereas negative velocity of muscle fibers indicates eccentric contraction. Fiber stretch velocity, outlined in figure 4.7, corresponds to simulation in which k_v = 0.1, is retained.

Thereafter, effects of k_p are explored. Simulations are, once more, generated. To effectively identify k_p, stretch velocities need to kept small to minimize interactions between velocity and position feedback. As a consequence, throughout analysis, k_v continued to be zero whereas l_d is set to 1.0. k_p is set to 0.0, 0.1, 0.5 and 1.0. The impingement of k_p on lumbar kinematics is clarified in figure 4.8.

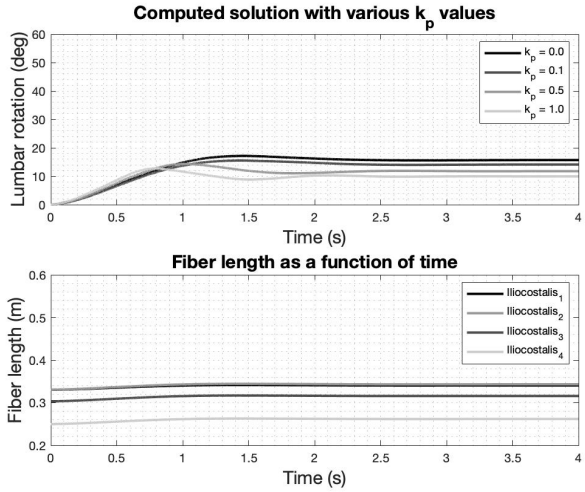

Figure 4.8: *top* figure illustrates rotation of $\mathcal{L}5 - \mathcal{S}1$ joint in sagittal plane with various k_p values. Reflexes are modeled as feedback from the muscle lengthening speed to muscle excitations, with reflex intensity modulated using k_p. Each contour represents lumbar rotation in which muscles generated force with a constant reflex gain. k_p is varied from 0.0 to 1.0. *Bottom* figure demonstrates muscle fiber length as a function of time.

Figure 4.8 depicts that as a consequence of increased k_p, admittance decreases, implicating a stiffer $\mathcal{L}5 - \mathcal{S}1$ joint. As evidenced in figure 4.8, muscles operate at constant fiber length after 1.5-s. It stands to reason that as a result, kinematic equilibrium is reached.

Lastly, effects of normalized fiber length are examined. l_d is interpreted as a ratio of the desired muscle length to the muscle neutral length. In an effort to explore impact on lumbar kinematics, l_d is set to 0.0, 0.1, 0.5 and 1.0 whereas k_p is set to 0.1. Additionally, at the point that k_v and k_p equal zero, reflex controller is deactivated. This does, however, not remain true on occasion that l_d equates zero. Therefore, a reference signal, proposing deactivated reflex controller, is added to figure 4.9.

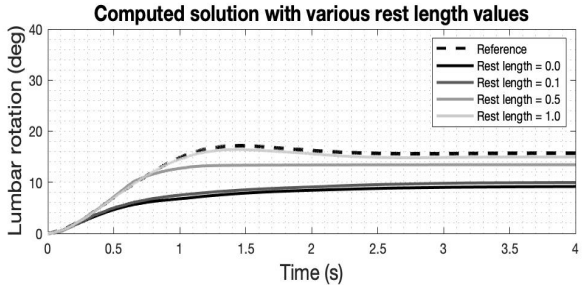

Figure 4.9: rotation of $\mathcal{L}5 - \mathcal{S}1$ joint in sagittal plane with various muscle rest length values. Reference signal (*dotted line*), proposes deactivated reflex controller. Reflexes are modeled as feedback from the muscle lengthening speed to muscle excitations, with reflex intensity modulated using l_d.

Figure 4.9 illustrates that alternating l_d affects lumbar kinematics. Similar to k_p, l_d possesses potential for stiffening purpose. In compliance with equation 3.2, selecting l_d = 0.0 alludes increased muscle activation. By reason, lumbar rotation is found to be smallest. Contrariwise, only minimal decrease in lumbar flexion is observed for l_d = 1.0.

In summary, large k_p and l_d precipitate decreased admittance. k_v contributes to declination in amplitude. In the ensuing paragraphs, l_d is set to 1.0. This implies desired muscle fiber length equals neutral muscle length. k_v and k_p are, on the contrary, estimated fitting experimental data.

4.6. Dynamic analysis: perturbations

Actual car seat, abutting pelvis, is not modelled. Aside from that, it is assumed the pelvis is the only body part in contact with the pretended car seat. As a consequence, external forces are applied directly to the pelvis. By multiplying platform accelerations engaged by Van Drunen et al. [10] with the fictitious pelvis mass of 10.000-kg, a force disturbance, is acquired. (Fig. 4.10).

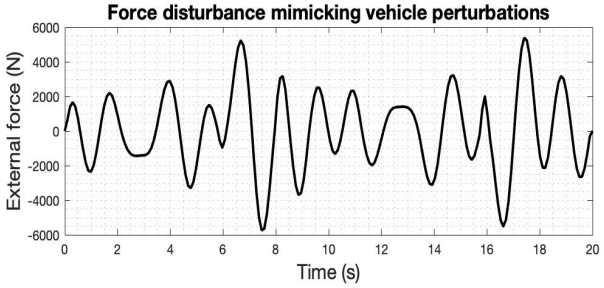

Figure 4.10: force disturbance mimicking vehicle perturbations. Positive forces constitute employment in anterior direction whereas negative forces constitute employment in posterior direction. Illustrated force disturbance is directly applied to pelvis.

From figure 4.10 it is readily apparent that the course of force disturbance, mimicking vehicle perturbations, is equivalent to the course of platform acceleration preliminarily exhibited in figure 3.5.

Above-mentioned force disturbance is applied to the pelvis and as a result, platform translation employed in the experiment from Van Drunen et al. [10], is simulated. Pelvis motion in comparison with platform motion is revealed in figure 4.11.

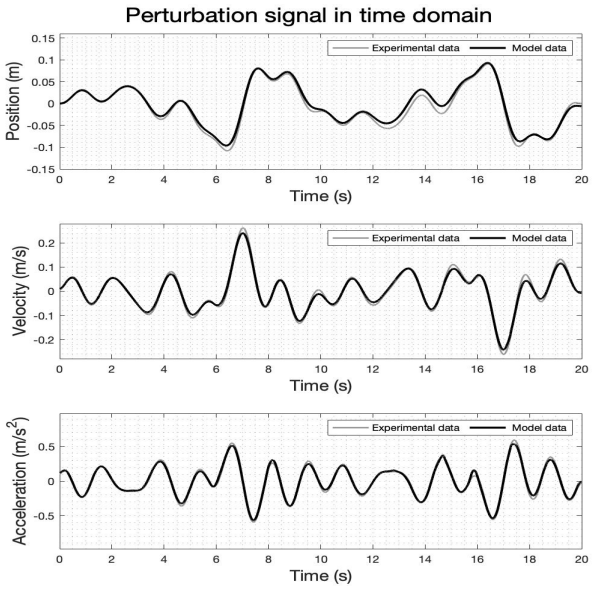

Figure 4.11: perturbation signal, imitating vehicle perturbations, in time domain. It can be learned that pelvis motion (*black lines*) resembles platform motion (*grey lines*) utilized in the experiment from Van Drunen et al. [10].

Figure 4.11 shows two conceivable trajectories. Black lines represent pelvis motion whereas grey lines represent platform translation. Pelvis motion resembles platform motion utilized by Van Drunen et al. [10]. Modest distinctions are, nonetheless, perceptible.

4.7. Dynamic analysis: experimental data

Heretofore, contributions of length-velocity feedback and muscle co-activation are explored. In an effort to verify that the model actually achieves its intended purpose, outcomes are validated with data from Van Drunen et al. [10]. As specified in the previous chapter, lumbar rotation is defined as the angle of $\mathcal{S}1$ and $\mathcal{L}1$ markers with the vertical axis. Nevertheless, significant differences in neutral body posture are inarguable. With the purpose of centering kinematics around the zero amplitude line, the offset is removed. As a consequence it is ensured all acquired experimental data starts at 0-deg rotation. Aforesaid procedure is followed for model outcomes.

As indicated in paragraph 3.5, experimental data is averaged. Firstly, data is averaged across repetitions and trials. Secondly, kinematics are averaged over subjects. Adequate result is revealed in figure 4.12.

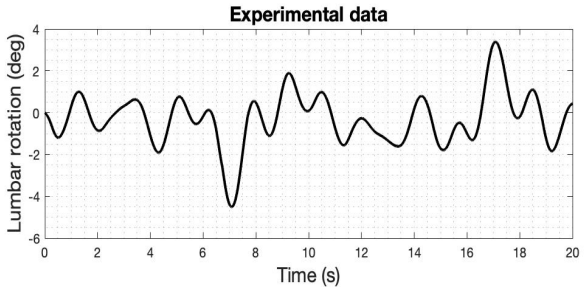

Figure 4.12: experimental lumbar kinematics after the appliance of averaging techniques. Positive rotation is affiliated with lumbar flexion whereas negative rotation is affiliated with lumbar extension. Indicated data is utilized for validation purpose.

On account of averaging, random fluctuations dissolve. As a consequence, it is conceivable to utilize experimental data, as exhibited in figure 4.12, for validation purpose. Effects of averaging across repetitions, trials and subjects are revealed in Appendix C.

4.8. Dynamic analysis: parameter estimation

By virtue of Gauss-Newton optimization, optimal k_v and k_p values are selected. Considering improper initial values can lead to local minima in lieu of global minima, adequate initials are important. Initial values are initiated by virtue of manual tuning. The optimization uses the reflexive control parameters as design variables. k_v and k_p are minorized by 0.001 and majorized by 1. Intending to explore contributions of reflexive control, the optimization algorithm is utilized under two scenarios. First scenario involves trunk settling in absence of force disturbance whereas second scenario involves car-passenger interaction.

4.8.1. Trunk settling

In the scenario of trunk settling, rotation of $\mathcal{L}1 - \mathcal{L}2$, $\mathcal{L}2 - \mathcal{L}3$, $\mathcal{L}3 - \mathcal{L}4$, $\mathcal{L}4 - \mathcal{L}5$ and $\mathcal{L}5 - \mathcal{S}1$ is totalled up. Thenceforward, the error between model kinematics and a reference signal corresponding to zero rotation, is minimized. Optimal control parameters associated with trunk settling are exhibited in table 4.2.

Muscle group	Parameters	Initial parameters	Final parameters
Sacrospinalis	Velocity gain k_v	0.0010	0.015
	Position gain k_p	0.0010	0.0012
Transversospinalis	Velocity gain k_v	0.0010	0.10
	Position gain k_p	0.0010	0.0019
Latissimus dorsi	Velocity gain k_v	0.0010	0.0016
	Position gain k_p	0.0010	0.0013
Quadratus laborum	Velocity gain k_v	0.0010	0.0014
	Position gain k_p	0.0010	0.059
Internal oblique	Velocity gain k_v	0.0010	0.0012
	Position gain k_p	0.0010	0.0012
External oblique	Velocity gain k_v	0.0010	0.020
	Position gain k_p	0.0010	0.053
Transversus abdominis	Velocity gain k_v	0.0010	0.0061
	Position gain k_p	0.0010	0.0012
Rectus abdominis	Velocity gain k_v	0.0010	0.037
	Position gain k_p	0.0010	0.0014
Psoas major	Velocity gain k_v	0.0010	0.0052
	Position gain k_p	0.0010	0.0013

Table 4.2: final reflexive control parameters in the event of trunk settling. Parameters are determined by means of Gauss-Newton algorithm. The objective function, describing the modelled lumbar rotation, is minimized. It is important to note that k_v and k_p are unitless quantities.

Table 4.2 demonstrates final reflexive control parameters in the situation of trunk settling. It is important to note, as depicted in conceptual scheme 3.2, initial controls proposing muscle co-activation, are employed to retain static posture. This alludes, regardless of reflexive contributions, static posture is heretofore preserved. Substantial reflexive control parameters are, therefore, implausible. Implied presumption is commensurate with literature. According to Hidler et al. [21], reflexive control parameters have shown to be low under normal conditions. Increased k_v and k_p have tendency to induce instability, known as muscle clonus [21].

Table 4.2 reveals that largest k_v and k_p are found for transversospinalis and quadratus laborum. This is attributable to the fact that at the instant reflexive control parameters are identical for all muscles, model flexes. For this reason, in conformity with optimization algorithm, spinal reflexive gains exceed abdominal reflexive gains.

4.8.2. Car-passenger interaction

In the scenario of car-passenger interaction, the error between model kinematics and experimentally measured kinematics is minimized. Reflexive control parameters illustrated in table 4.2 are incapable of stabilizing the model in the event of external forces. Thus, reflexive control parameters ought to be revised. Reflexive control parameters in the event of car-passenger interaction are presented in table 4.3.

Muscle group	Parameters	Initial parameters	Final parameters
Sacrospinalis	Velocity gain k_v	0.10	0.13
	Position gain k_p	0.10	0.20
Transversospinalis	Velocity gain k_v	0.10	0.14
	Position gain k_p	0.10	0.21
Latissimus dorsi	Velocity gain k_v	0.70	0.70
	Position gain k_p	0.10	0.20
Quadratus laborum	Velocity gain k_v	0.70	0.70
	Position gain k_p	0.10	0.25
Internal oblique	Velocity gain k_v	0.10	0.011
	Position gain k_p	0.10	0.16
External oblique	Velocity gain k_v	0.10	0.16
	Position gain k_p	0.010	0.011
Transversus abdominis	Velocity gain k_v	0.010	0.016
	Position gain k_p	0.010	0.011
Rectus abdominis	Velocity gain k_v	0.10	0.17
	Position gain k_p	0.010	0.011
Psoas major	Velocity gain k_v	0.010	0.013
	Position gain k_p	0.010	0.011

Table 4.3: final reflexive control parameters in the event of car-passenger interaction. Parameters are determined by means of Gauss-Newton algorithm. The error between model kinematics and experimentally measured kinematics is minimized. It is important to note that k_p and k_v are uniteless quantities.

Table 4.2 and 4.3 transpire that control parameters vary with conditions. As a matter of fact, it is acknowledged humans can modulate their reflexive settings to the characteristics of disturbances [10]. On the occasion that perturbation is enforced, additional resistance is indispensable. Supplementary stiffness is achieved by rised k_v and k_p. It is remarkable, similar to settling scenario, largest reflexive control parameters are found for spinal muscle groups.

4.9. Dynamic analysis: validation

Ongoing paragraph debates lumbar kinematics in presence of force disturbance. Summarily, the model retains 6-DOF being translational pelvis motion which is externally prescribed, and flexion at the 5 lumbar joints being $\mathcal{L}1-\mathcal{L}2$, $\mathcal{L}2-\mathcal{L}3$, $\mathcal{L}3-\mathcal{L}4$, $\mathcal{L}4-\mathcal{L}5$ and $\mathcal{L}5-\mathcal{S}1$. A fade-in period of 2-$s$ is applied so as to minimize transient behaviour and to prevent abrupt pelvis motion. For the purpose of characterizing lumbar rotation, rotation of $\mathcal{L}1-\mathcal{L}2$, $\mathcal{L}2-\mathcal{L}3$, $\mathcal{L}3-\mathcal{L}4$, $\mathcal{L}4-\mathcal{L}5$ and $\mathcal{L}5-\mathcal{S}1$ is totalized. A representation of the angle of $\mathcal{S}1$ and $\mathcal{L}1$ with the vertical axis is, hereby, specified. Finally, validity of the model is evaluated in time domain by means of the VAF. Dynamic behaviour of the system, as a function of frequency, is described by the FRF.

4.9.1. Time domain analysis

Minimal muscle activation level of 0.020, yielding elevated joint stiffness, is adapted. So as to fit experimental data, intervertebral stiffness and damping are set to 125 and 7.5-Nm/rad, respectively.

As presented in figure 4.13, intrinsic properties alone are incapable of stabilizing the spine in presence of force disturbance. Thus, control correction signals, computed from *Muscle Fiber Stretch Controller*, are fundamental.

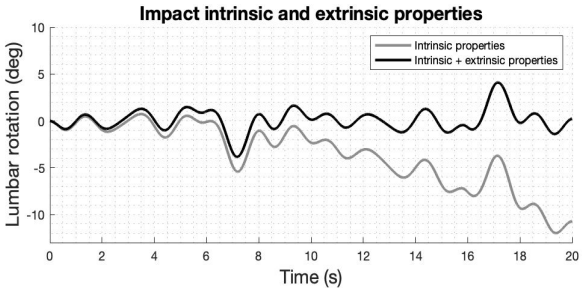

Figure 4.13: impact of intrinsic and extrinsic properties on lumbar kinematics. Intervertebral joint properties and muscle co-activation (*grey line*) are unable to provide lumbar stability in presence of force disturbance. Supplemental resistance is acquired by virtue of extrinsic muscle properties (*black line*).

Figure 4.13 elucidates the model tends to move away from its original equilibrium state. The equilibrium state of the model is, therefore, said to be unstable. Intrinsic properties together with extrinsic properties are, on the contrary, able to maintain spinal stability.

At this point in analysis, intrinsic properties in conjunction with final reflexive control parameters as presented in table 4.3, are embedded in the model. Final model result, in contradistinction to experimental data, is revealed in figure 4.14.

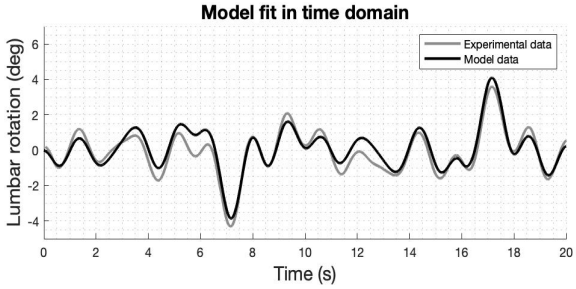

Figure 4.14: model fit in time domain. Figure exhibits model kinematics (*black line*) as opposed to experimental kinematics (*grey line*) during 1-Hz perturbation bandwidth.

Figure 4.14 reveals that model shows a reasonable time domain fit. By the utility of Gauss-Newton optimization, model fit improves and ultimately, the OpenSim model explicates 86.00% of the dispersion. As opposed to experimental kinematics, model is allegedly damped.

4.9.2. Frequency domain analysis

Frequency domain measures provide detail into kinematics responses by decomposing model responses into specific frequencies of motion. Figure 4.15 displays kinematic FRF across a 20-s trial. Frequency domain dependent variables include SD of 95% confidence interval on the mean values. Gain and phase are calculated from Fourier transforms and indicate relative output at each frequency. Gain of 1 and phase of 0 express perfect alignment of kinematic response to perturbation in absence of lead or lag in timing. Gain < 1 suggests diminished sensitivity to perturbations and negative phase suggests a lag in responsiveness at particular frequencies.

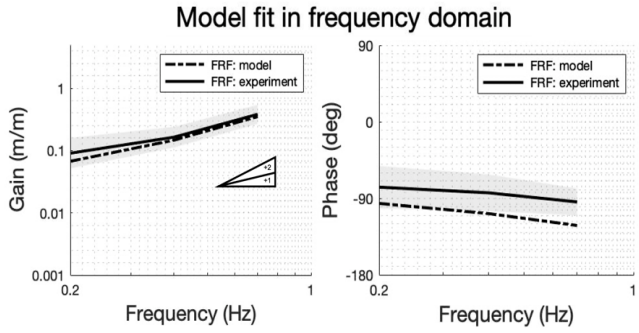

Figure 4.15: FRF of lumbar kinematics during 1-Hz perturbation bandwidth. Model kinematics (*dotted lines*) and experimental kinematics (*solid lines*) are described by lumbar rotation in sagittal plane. Gain (amplitude difference) and phase (time shift) illustrate the transformation of the input signal to the output signal. *Triangle* is given as reference of the slope of the gains indicating stiffness (+2) and damping (+1) [10].

Figure 4.15 shows that gain increases at higher frequency points, indicating an increased responsiveness to perturbation. Phases appear to be lower at higher stimulus frequencies, indicating phase lag in responses at designated frequencies [15]. Interestingly, model expresses increased phase lag. The implied can be ascribed to damping.

Van Drunen et al. [10] revealed that kinematic FRF resembles the characteristics of a second-order system with natural frequency around 1-Hz. As revealed in figure 4.15, below natural frequency, gain slopes between $+1$ and $+2$ are found, indicating dominant behaviour of intrinsic stiffness, damping and reflexes [10].

5

Discussion

The minute a car starts moving and is subject to accelerations and decelerations, the driver is exposed to various forces. The goal of this research was to simulate car-passenger interaction intending to understand how movements of self-driving cars are transmitted to passengers and how passengers cope with perturbations affecting passenger's balance.

5.1. Static analysis

Isometric strength outcomes, exemplified in figure 4.2, show that model predictions correlate with in vivo measurements. Isometric strength of several individual muscles was enhanced. Resultantly, isometric strength outcomes in the present study were found to be superior to isometric strength outcomes from Schmid et al. [43]. It is worthy to note, Schmid et al. [43] made use of actuators to simulate restriction of the pelvis whereas in the study, pelvis joint was locked. Furthermore, to enhance simulation time throughout static optimization, hip, knee, ankle, elbow and wrist joints were locked. Be that as it may, difference in methodology did not give rise to incompatible outcomes.

Nonetheless, several limitations should be considered. First of all, in order to facilitate maximal isometric flexion force in sagittal plane, Schmid et al. [43] applied an external force to the sternum. As previously described in section 2.2.1, Schmid et al. [43] modelled sternum as claviculae, scapulae and arms. On account of assigning an external force to sternum, muscles featuring attachment points to specified bodies, got activated. It was brought to light that throughout static analysis, neck muscles reached their upper bound. Accordingly, the *Static Optimization Tool* threw an exception constraints were violated. As an alternative, external loads were applied to $\mathcal{T}6$ and $\mathcal{T}7$. By virtue of applying external loads to $\mathcal{T}6$ and $\mathcal{T}7$ in place of the sternum, overall neck muscle activation decreased. Maximal isometric flexion, on the contrary, increased from 880-N to 900-N.

Throughout analysis, a subject-specific OpenSim model of an 18-year old male was used. In the event of scaling the model, it is difficult to minimize the marker error of the model. It is, therefore, arduous to generalize results to other subjects. For validation purposes, isometric strength data of an 18-year old male, was preferred. Isometric strength outcomes of 18-year old males were, however, not found in literature.

5.2. Dynamic analysis

The effects of passive joint properties were parametrically examined for a static posture. Figure 4.5 reveals that on account of intervertebral stiffness, additional joint stiffness is provided. Findings were in consonance with literature. The fact is that stiffness plays a critical role on muscle forces required for equilibrium [30]. The passive dynamic element representing intervertebral damping is associated with decreased postural sway. It may be collectively interesting that increased postural sway is well documented in patients suffering low-back pain [30]. In short, intervertebral stiffness and damping parameters generated an increased effective torsional stiffness and provided additional protection.

Muscle co-activation was modelled using the *Static Optimization Tool* which sought to estimate muscle activations that satisfied static posture. Indicated optimization is fast, nonetheless, imprecise. Figure 4.6 reveals that, as a consequence of muscle co-activation, larger joint stiffness is generated. Additionally, figure 4.6 shows that in spite of postural activity, a lumbar flexion angle of 2-deg is perceptible. With an eye on further reducing lumbar flexion, lower bound for muscle activation level was increased. It was recognized that minimal muscle activation levels > 0.020 did not impose renovated results. Nevertheless, co-activation remains a challenging feature to include in musculoskeletal models and may be improved by extracting optimization objective functions from experimental data [33]. Components of an objective function must, however, be known before fitting to experimental data.

Muscle fiber length and contraction velocity are sensed by the muscle spindle. The gains of the proprioceptive feedback loops are limited by stability requirements [50]. Due to length-velocity feedback a larger range of impedance levels can be obtained [31]. Figure 4.7 and 4.8 exemplify large k_p and l_d precipitate decreased admittance whereas k_v contributes to declination in amplitude.

With the aid of a mechanical force disturbance, car-passenger interaction was simulated. Table 4.2 and table 4.3 illustrate that in the eventuality of force disturbance reflexive gains are increased. This is in conformity with literature inasmuch as increased effective trunk stiffness is required to maintain stability of the system in presence of force disturbance [12].

Raw perturbation signal, acquired from Van Drunen et al. [10], was filtered by dint of a low pass filter with a passband frequency of 2-Hz. It is, however, feasible Van Drunen et al. [10] followed distinct approach. Pelvis motion was, however, not fully compatible with platform translation. In spite of that, lumbar kinematics showed an adequate time domain model fit (VAF = 86.00%). Thus, the model is able to describe kinematic behaviour of the lumbar spine.

Decomposing perturbation and lumbar kinematics in frequency domain is particularly helpful to address the question of specificity. In response to sagittal plane stimuli, typical patterns of gain and phase across frequencies involve gain increases from 0.01 to 0.8-Hz followed by gain decreases at frequencies above 1-Hz [15][37]. Phases typically show more lag with increasing frequency [15][37]. The same general behaviour is described by the OpenSim model (Fig. 4.15). It can be clearly seen in figure 4.15, model expresses increased phase lag. Designated phenomenon is ascribable to the model being damped.

In spite of that, a handful of aspects should be debated. First, it is noteworthy to mention that OpenSim can generate simulations surpassing real-time. In an attempt to reduce computation time, tendon slack length, by means of trial and error, was adjusted. Resulting muscle behaviour was, however, sensitive to parameter changes. As a consequence, it was revealed that estimated values of tendon slack length had significant effect on modelling. It remains arguable whether assigned tendon slack length values are ideal. Furthermore, despite the diminution of the number of integrator steps, forward dynamics simulation remained rather stiff. Improper inertial parameters could contribute to increased simulation time as they play an important contribution to dynamic analysis. Schmid et al. [43] inquired into static analysis and regarded inertial properties as less crucial. Inertia of sternum, ribs, claviculae and scapulae appeared to be less than 0.000009-kg/m^2. The reliability of incorporated inertial parameters is, therefore, questionable. Considering the fact designated bodies were immovable throughout dynamic analysis, lumbar stabilization outcomes were not affected. However, to improve suitability for full-body analysis, inertial parameters for body segments should be reconsidered. A feasible approach to estimate inertial parameters consists in using identification techniques. Identification techniques are gleaned from model dynamics and experimental data about motion and external reaction forces [53].

Second, to make preparations for dynamic analysis, the model from Schmid et al. [43] was conventionalized. Muscles that did not contribute to lumbar stabilization were enabled. In other words, neck, peroneus, gastrocnemius, trapezius and serratus anterior were deleted form the XML file. Moreover, spinal joints comprised 1-DOF rather than 3-DOF. For that reason, it should be taken into account that the model did not accurately reflect reality.

Third, intervertebral rotational joint stiffness, implemented by means of a *Bushing Force*, is limited to linear stiffness and linear damping. Intervertebral joint stiffness is, however, known to be nonlinear and affected by factors such as preload. Therefore, additional work is needed to examine the effects of intervertebral stiffness in non-sagittal plane motions.

In contrast to Demers et al. [9], solely k_v and k_p were optimized whereas l_d was set to 1.0. Considering equalizing reflexive control parameters of muscles resulted in substandard results, muscles were assembled in a group in which muscles shared identical k_v and k_p. The implied procedure was, in terms of parameter tuning, computationally demanding. In the fullness of time, MATLAB solved the optimization problem in ± 70-h.

On top of that, static optimization, as implemented in OpenSim, was used to estimate muscle co-activation for postural activity. Static optimization accounts for muscle force-length-velocity. Passive force contributions are, on the contrary, disregarded. Moreover, the static optimization problem is linear in its design variables [34]. Despite the fact that the characteristic curves that describe muscle forces are non-linear, muscle activations are the only design variables in the problem and appear linearly in the muscle-generated joint moment equations [8]. An optimization problem selectively incorporating linear constraints is beneficial since problems can be solved more efficiently. Furthermore, OpenSim only provides one type of cost function for optimization. As an alternative, Macintosh et al. [24] used a muscle stress squared criterion and came up with an EMG-constrained static optimization solution. Macintosh et al. [24] discovered that assisted neural EMG solution, compared to static optimization, produced greater co-contraction.

Lastly, emphasis primarily lay on the kinematic response of the lumbar spine. By virtue of averaging kinematic responses of six subjects, inter and intra-individual variability were considered. Be that as it may, Schmid et al. [43] developed a model of an 18-year old male. Studies showed that due natural aging the musculoskeletal system becomes stiffer [26]. Hence, aging impacts joint kinematics. In view of the fact that model outcomes were tuned towards experimental data, it may be erroneous to validate subject-specific model outcomes with generic data.

6

Conclusion and recommendations

6.1. Conclusion

Referring to static analysis, the predicted isometric trunk strength correlated with in vivo measurements. The model comprises sufficient strength in lumbar forward, rearward and lateral flexion and therefore has the potential to serve as a basis for dynamic analysis.

When aiming at simulations of car-passenger interaction, passive joint properties, length-velocity feedback and postural activity are embedded in the model. By means of intervertebral joint properties and muscle co-activation, static posture, in absence of force disturbance, is preserved. Intrinsic properties alone can, however, not be relied upon to generate enough torque to compensate for the applied force disturbance. Supplementary resistance is achieved by raised reflexive control gains. Assembling designated model for dynamic analysis required extensive model calibration. Model parameters are adjusted such that the model closely matched experimental kinematics. Designated procedure was time and computationally expensive. Given the simplifications of the present model, the results agree well with outcomes from Van Drunen et al. [10].

6.2. Future research

Current research concentrated on lumbar kinematics. However, to be confident in modelling results, estimated muscle activity should be examined as well. In defiance of validated lumbar kinematics, it is undisclosed muscle activity assimilates with experimentally measured EMG. It is, therefore, conceivable muscles do not possess the activity they supposed to have. Further research should address this hypothesis in more detail. On that account, surface EMG of back muscles, with preference of an 18-year old male, should be assessed. It is important to note that EMG is not an exact measure of the underlying muscle activity.

Dissimilar from Van Drunen et al. [10], present study does not investigate the effect of bandwidth on lumbar stabilization. Van Drunen et al. [10] stated that adjusting perturbation bandwidth resulted in modulation of lumbar motor control. Moreover, to investigate broader range of reflexive modulation, rotational perturbations may be considered. Postural disturbances characterized by small rotations result in high reflexive involvement [13]. Therefore, it may be interesting to identify these effects.

In the present study, vision is neglected. Vision is related to a strategy decreasing overall stiffness by a decrease in intrinsic stiffness [10]. Direct visual feedback contributes at low frequencies since visual processing time results in a long latency time delay. Future research may consider visual feedback. For the purpose of including vision, it is conceivable to include an internal feedback path [30]. Designated feedback path provides predictions of kinematics and the sensory consequences of those actions to yield an instantaneous prediction error. Consequently, a set of muscle activations through the action of a neural feedback controller is introduced.

Inertial parameters of body segments are necessary parameters to perform dynamic analysis of human movement. Seeing that Schmid et al. [43] actualized a static analysis, for future research, inertial parameters may be revised.

7

References

1. Ackland, D. C., Lin, Y. C., Pandy, M. G. (2012). Sensitivity of model predictions of muscle function to changes in moment arms and muscle-tendon properties: a Monte-Carlo analysis. Journal of biomechanics, 45(8), 1463–1471. https://doi.org/10.1016/j.jbiomech.2012.02.023

2. Al-Mbaideen, A. (2019). Application of Moving Average Filter for the Quantitative Analysis of the NIR Spectra. Journal Of Analytical Chemistry, 74(7), 686-692. doi: 10.1134/s1061934819070013

3. Aminoff, M. J., Boller, F., Swaab, D. F. (2003). Handbook of Clinical Neurology. Elsevier Gezondheidszorg.

4. Arnold, E. M., Hamner, S. R., Seth, A., Millard, M., Delp, S. L. (2013). How muscle fiber lengths and velocities affect muscle force generation as humans walk and run at different speeds. Journal of Experimental Biology. https://doi.org/10.1242/jeb.075697

5. Buchanan, T. S., Lloyd, D. G., Manal, K., Besier, T. F. (2004). Neuromusculoskeletal modeling: estimation of muscle forces and joint moments and movements from measurements of neural command. Journal of applied biomechanics, 20(4), 367–395. https://doi.org/10.1123/jab.20.4.367

6. Christophy, M., Curtin, M., Faruk Senan, N., Lotz, J., O'Reilly, O. (2012). On the modeling of the intervertebral joint in multibody models for the spine. Multibody System Dynamics, 30(4), 413-432. doi: 10.1007/s11044-012-9331-x

7. Dean J. C. (2013). Proprioceptive feedback and preferred patterns of human movement. Exercise and sport sciences reviews, 41(1), 36–43. https://doi.org/10.1097/JES.0b013e3182724bb0

8. Delp, S., Anderson, F., Arnold, A., Loan, P., Habib, A., John, C. et al. (2007). OpenSim: Open-Source Software to Create and Analyze Dynamic Simulations of Movement. IEEE Transactions On Biomedical Engineering, 54(11), 1940-1950. doi: 10.1109/tbme.2007.901024

9. DeMers, M., Hicks, J., Delp, S. (2017). Preparatory co-activation of the ankle muscles may prevent ankle inversion injuries. Journal Of Biomechanics, 52, 17-23. doi: 10.1016/j.jbiomech.2016.11.002

10. van Drunen, P., Koumans, Y., van der Helm, F., van Dieën, J., Happee, R. (2015). Modulation of intrinsic and reflexive contributions to low-back stabilization due to vision, task instruction, and perturbation bandwidth. Experimental Brain Research, 233(3), 735-749. doi: 10.1007/s00221-014-4151-2

11. Fehrenbach, J., De Gournay, F. (2019). Shape optimizationviaa levelset and a Gauss-Newton method. ESAIM: Control, Optimisation and Calculus of Variations, 25, 3. https://doi.org/10.1051/cocv/2017014

12. Franklin, T., Granata, K. (2007). Role of reflex gain and reflex delay in spinal stability—A dynamic simulation. Journal Of Biomechanics, 40(8), 1762-1767. doi: 10.1016/j.jbiomech.2006.08.007

13. Freyler, K., Gollhofer, A., Colin, R., Brüderlin, U., Ritzmann, R. (2015). Reactive Balance Control in Response to Perturbation in Unilateral Stance: Interaction Effects of Direction, Displacement and Velocity on Compensatory Neuromuscular and Kinematic Responses. PloS one, 10(12), e0144529. https://doi.org/10.1371/journal.pone.0144529

14. Frey-Law, L. A., Avin, K. G. (2013). Muscle coactivation: a generalized or localized motor control strategy?. Muscle nerve, 48(4), 578–585. https://doi.org/10.1002/mus.23801

15. Goodworth, A. D., Peterka, R. J. (2018). Identifying mechanisms of stance control: A single stimulus multiple output model-fit approach. Journal of neuroscience methods, 296, 44–56. https://doi.org/10.1016/j.jneumeth.2017.12.015

16. Grace Gaerlan, M., Alpert, P. T., Cross, C., Louis, M., Kowalski, S. (2012). Postural balance in young adults: the role of visual, vestibular and somatosensory systems. Journal of the American Academy of Nurse Practitioners, 24(6), 375–381. https://doi.org/10.1111/j.1745-7599.2012.00699.x

17. Hagio, K., Obata, H., Nakazawa, K. (2018). Effects of breathing movement on the reduction of postural sway during postural-cognitive dual tasking. PloS one, 13(5), e0197385. https://doi.org/10.1371/journal.pone.0197385

18. Heenan, M., Scheidt, R., Woo, D., Beardsley, S. (2014). Intention tremor and deficits of sensory feedback control in multiple sclerosis: a pilot study. Journal Of Neuroengineering And Rehabilitation, 11(1). doi: 10.1186/1743-0003-11-170

19. Hernandez M. (2014). Gauss-Newton inspired preconditioned optimization in large deformation diffeomorphic metric mapping. Physics in medicine and biology, 59(20), 6085–6115. https://doi.org/10.1088/0031-9155/59/20/6085

20. Hicks, J. (2018). CMC Best Practices - OpenSim 3.3 Documentation. OpenSim 3.3 Documentation. Consulted on 7 juni 2022, from https://simtk-confluence.stanford.edu:8443/display/OpenSim33/CMC+Best+Practices

21. Hidler, J., Rymer, W. (1999). A simulation study of reflex instability in spasticity: origins of clonus. IEEE Transactions on Rehabilitation Engineering, 7(3), 327–340. https://doi.org/10.1109/86.788469

22. Jovanovic, K., Vranic, J., Miljkovic, N. (2015). Hill's and Huxley's muscle models - tools for simulations in biomechanics. Serbian Journal Of Electrical Engineering, 12(1), 53-67. doi: 10.2298/sjee1501053j

23. Knarr, B. A., Zeni, J. A., Higginson, J. S. (2012). Comparison of electromyography and joint moment as indicators of co-contraction. Journal of Electromyography and Kinesiology, 22(4), 607–611. https://doi.org/10.1016/j.jelekin.2012.02.001

24. Lee, N., Kang, H., Shin, G. (2015). Use of antagonist muscle EMG in the assessment of neuromuscular health of the low back. Journal of physiological anthropology, 34(1), 18. https://doi.org/10.1186/s40101-015-0055-5

25. Mansouri, M., Reinbolt, J. A. (2012). A platform for dynamic simulation and control of movement based on OpenSim and MATLAB. Journal of biomechanics, 45(8), 1517–1521. https://doi.org/10.1016/j.jbiomech.2012.03.016

26. Marcucci, L., Reggiani, C. (2020). Increase of resting muscle stiffness, a less considered component of age-related skeletal muscle impairment. European journal of translational myology, 30(2), 8982. https://doi.org/10.4081/ejtm.2019.8982

27. Markolf, K. (1972), "Deformation of the Thoracolumbar Intervertebral Joints in Response to External Loads: A Biomechanical Study Using Autopsy Material," J. Bone Jt. Surg., 54 (3), pp. 511—533

28. Massion J. (1994). Postural control system. Current opinion in neurobiology, 4(6), 877–887. https://doi.org/10.1016/0959-4388(94)90137-6

29. McErlain-Naylor, S. A., King, M. A., Felton, P. J. (2021). A Review of Forward-Dynamics Simulation Models for Predicting Optimal Technique in Maximal Effort Sporting Movements. Applied Sciences, 11(4), 1450. https://doi.org/10.3390/app11041450

30. Meng, X., Bruno, A., Cheng, B., Wang, W., Bouxsein, M., Anderson, D. (2015). Incorporating Six Degree-of-Freedom Intervertebral Joint Stiffness in a Lumbar Spine Musculoskeletal Model—Method and Performance in Flexed Postures. Journal Of Biomechanical Engineering, 137(10). doi: 10.1115/1.4031417

31. Menotti, F., Labanca, L., Laudani, L., Giombini, A., Pigozzi, F., Macaluso, A. (2015). Activation of Neck and Low-Back Muscles Is Reduced with the Use of a Neck Balance System Together with a Lumbar Support in Urban Drivers. PLOS ONE, 10(10), e0141031. https://doi.org/10.1371/journal.pone.0141031

32. Mirakhorlo, M., Kluft, N., Desai, R., Cvetković, M., Irmak, T., Shyrokau, B., Happee, R. Simulating 3D Human Postural Stabilization in Vibration and Dynamic Driving. Preprints 2022, 2022050307. doi: 10.20944/preprints202205.0307.v1

33. Mortensen, J., Trkov, M., Merryweather, A. (2018). Exploring novel objective functions for simulating muscle coactivation in the neck. Journal of biomechanics, 71, 127–134. https://doi.org/10.1016/j.jbiomech.2018.01.030

34. Neptune, R. R., McGowan, C. P., Kautz, S. A. (2009). Forward dynamics simulations provide insight into muscle mechanical work during human locomotion. Exercise and sport sciences reviews, 37(4), 203–210. https://doi.org/10.1097/JES.0b013e3181b7ea29

35. Paalanne, N., Korpelainen, R., Taimela, S., Remes, J., Mutanen, P., Karppinen, J. (2008). Isometric Trunk Muscle Strength and Body Sway in Relation to Low Back Pain in Young Adults. Spine, 33(13), E435-E441. doi: 10.1097/brs.0b013e318175c2c7

36. Panjabi, M. (1992). The Stabilizing System of the Spine. Part I. Function, Dysfunction, Adaptation, and Enhancement. Journal Of Spinal Disorders, 5(4), 383-389. doi: 10.1097/00002517-199212000-00001

37. Peterka R. J. (2002). Sensorimotor integration in human postural control. Journal of neurophysiology, 88(3), 1097–1118. https://doi.org/10.1152/jn.2002.88.3.1097

38. Prilutsky, B. I., Zatsiorsky, V. M. (2002). Optimization-based models of muscle coordination. Exercise and sport sciences reviews, 30(1), 32–38. https://doi.org/10.1097/00003677-200201000-00007

39. Rasman, B. G., Forbes, P. A., Tisserand, R., Blouin, J. S. (2018). Sensorimotor Manipulations of the Balance Control Loop-Beyond Imposed External Perturbations. Frontiers in neurology, 9, 899. https://doi.org/10.3389/fneur.2018.00899

40. Riemann, B. L., Lephart, S. M. (2002). The sensorimotor system, part I: the physiologic basis of functional joint stability. Journal of athletic training, 37(1), 71–79.

41. Roberts, T. J., Gabaldón, A. M. (2008). Interpreting muscle function from EMG: lessons learned from direct measurements of muscle force. Integrative and comparative biology, 48(2), 312–320. https://doi.org/10.1093/icb/icn056

42. Salmond, L. H., Davidson, A. D., Charles, S. K. (2017). Proximal-distal differences in movement smoothness reflect differences in biomechanics. Journal of neurophysiology, 117(3), 1239–1257. https://doi.org/10.1152/jn.00712.2015

43. Schmid, S., Burkhart, K., Allaire, B., Grindle, D., Anderson, D. (2020). Musculoskeletal full-body models including a detailed thoracolumbar spine for children and adolescents aged 6–18 years. Journal Of Biomechanics, 102, 109305. doi: 10.1016/j.jbiomech.2019.07.049

44. Schwartz A. B. (2016). Movement: How the Brain Communicates with the World. Cell, 164(6), 1122–1135. https://doi.org/10.1016/j.cell.2016.02.038

45. Sell, T., Lephart, S. (2017). Noyes' Knee Disorders. Medicine Science In Sports Exercise, 49(7), 1499. doi: 10.1249/mss.0000000000001323

46. Seth, A., Hicks, J., Uchida, T., Habib, A., Dembia, C., Dunne, J. et al. (2018). OpenSim: Simulating musculoskeletal dynamics and neuromuscular control to study human and animal movement. PLOS Computational Biology, 14(7), e1006223. doi: 10.1371/journal.pcbi.1006223

47. Stifani, N. (2014). Motor neurons and the generation of spinal motor neuron diversity. Frontiers In Cellular Neuroscience, 8. doi: 10.3389/fncel.2014.00293

48. Thelen, D. (2003). Adjustment of Muscle Mechanics Model Parameters to Simulate Dynamic Contractions in Older Adults. Journal Of Biomechanical Engineering, 125(1), 70-77. doi: 10.1115/1.1531112

49. Thomas, K., Lee, R. Y. W. (2000). Fatigue of abdominal and paraspinal muscles during sustained loading of the trunk in the coronal plane. Archives of Physical Medicine and Rehabilitation, 81(7), 916– 920. https://doi.org/10.1053/apmr.2000.5577

50. Tuthill, J., Azim, E. (2018). Proprioception. Current Biology, 28(5), R194-R203. doi: 10.1016/j.cub.2018.01.064

51. Ulbig, A., Borsche, T. S., Andersson, G. (2014). Impact of Low Rotational Inertia on Power System Stability and Operation. IFAC Proceedings Volumes, 47(3), 7290–7297. https://doi.org/10.3182/20140824-6-za-1003.02615

52. Vaes, P., Duquet, W., Van Gheluwe, B. (2002). Peroneal Reaction Times and Eversion Motor Response in Healthy and Unstable Ankles. Journal of athletic training, 37(4), 475–480.

53. Verheul, J., Warmenhoven, J., Lisboa, P., Gregson, W., Vanrenterghem, J., Robinson, M. A. (2019). Identifying generalised segmental acceleration patterns that contribute to ground reaction force features across different running tasks. Journal of science and medicine in sport, 22(12), 1355–1360. https://doi.org/10.1016/j.jsams.2019.07.006

54. Weiss, P. L., Kearney, R. E., Hunter, I. W. (1986). Position dependence of stretch reflex dynamics at the human ankle. Experimental brain research, 63(1), 49–59. https://doi.org/10.1007/BF00235645

55. Wilson, A., Lichtwark, G. (2011). The anatomical arrangement of muscle and tendon enhances limb versatility and locomotor performance. Philosophical transactions of the Royal Society of London. Series B, Biological sciences, 366(1570), 1540–1553. https://doi.org/10.1098/rstb.2010.0361

A

Static analysis

A.1. Static analysis: maximal isometric force

Muscle	Old isometric force value (N)	New isometric force value (N)
Rect-abd	661.52	701.52
IO1	197.95	207.95
IO2	203.72	213.72
IO3	193.18	203.18
IO4	236.96	246.96
IO5	206.38	216.38
IO6	181.35	191.35
E0-R5	45.97	55.97
E0-R6	58.84	68.84
E0-R7	126.09	136.09
E0-R8	173.63	183.63
E0-R9	199.68	209.68
E0-R10	139.85	149.85
E0-R11	138.87	148.87
E0-R12	151.93	161.93
TR1	161.92	171.92
TR2	57.69	67.69
TR3	57.00	67.69
TR4	57.00	67.69
TR5	200.14	360.14
LT-PT-T1	335.89	475.89
LT-PT-T2	240.66	390.66
LT-PT-T3	172.50	322.50
LT-PT-T4	60.57	210.57
LT-PT-T5	57.01	157.01
LT-PT-T6	81.40	181.40
LT-PT-T7	79.70	179.70

Muscle	Old isometric force value (N)	New isometric force value (N)
LT-PT-T8	120.46	270.46
LT-PT-T9	139.43	289.43
LT-PL-L1	106.15	256.15
LT-PL-L2	118.38	258.38
LT-PL-L3	121.28	271.28
LT-PL-L5	157.79	307.79
SER-ANT-2-1	173.78	193.78
SER-ANT-3-1	150.06	160.06
SER-ANT-4-1	208.25	218.25
SER-ANT-5-1	162.14	172.14
MF-M1S	71.19	231.19
MF-M2S	44.47	54.47
MF-M3S	73.72	83.72
MF-M4S	121.07	151.07
MF-M1T-1	61.96	71.96
MF-M1T-2	49.72	59.72
MF-M2T-1	47.46	57.46
MF-M2T-2	135.89	145.89
MF-M3T-1	100.97	140.97
MF-M3T-2	89.97	99.97
MF-M4T-1	110.11	140.11
Multifidus-L1-T11	221.12	391.12
Multifidus-L2-T12	209.35	379.35
Multifidus-T6-T4	253.66	283.66
Multifidus-T7-T5	231.54	251.54
Multifidus-T8-T6	188.96	248.96
Multifidus-T11-T9	209.50	319.50

Table A.1: overview of modified maximal isometric force values. The *Static Optimization Tool* throws an exception at the instant constraints are violated. Subsequently, OpenSim suggests to append additional forces to reduce the reported acceleration constraints. In the research, maximal isometric force of the reported muscles is increased and as a result, maximal isometric trunk strength is enforced.

A.2. Static analysis: muscle activation

Analysis	Muscle group	Muscles
Maximal extension in sagittal plane	Transversospinalis Sacrospinalis Transversus abdominis	IL-L1, IL-L2, IL-L4, LT-PT-T9, LT-PT-T10, LT-PT-T11, LT-PT-R9, LT-PT-R10, LT-PT-R11, LT-PL-L5, LT-PL-L4, LT-PL-L3, LT-PL-L2, LT-PL-L1, MF-M3t-1, MF-M3t-2, MF-M3t-3, MF-M4t-2, MF-M4t-3, MF-M5s, MF-M5t-1, MF-M5t-2, MF-M5t-3, MF-M5-laminar, Multi-L2-T12, TR5
Maximal flexion in sagittal plane	Psoas major Rectus abdominis Internal oblique External oblique Transversus abdominis Latissimus dorsi	PS-L1-VB, PS-L1-L2-IVD, PS-L2-L3-IVD, PS-L3-L4-IVD, Rect-abd, LT-PT-T1, LT-PT-T2, E05, E06, E07, E08, LD-T12, LD-T11, LD-T10, LD-T9, LD-T8, LD-T7, Multi-T12-T10, Multi-T11-T9, Multis-T7-T5, Multi-T6-T4, Serr-21, Serr-91, TR1, TR2, TR3, EXT-IS2-3, EXT-IS2-5, EXT-IS2-7, EXT-IS3-3, EXT-IS3-5, EXT-IS3-7, EXT-IS4-1, EXT-IS4-3, EXT-IS4-5, EXT-IS4-7, EXT-IS5-1, EXT-IS5-3, EXT-IS5-5, EXT-IS5-7, EXT-IS6-1, EXT-IS6-3, EXT-IS6-5, EXT-I46-7, EXT-IS7-1, EXT-IS7-3, EXT-IS8-1, EXT-IS8-3, EXT-IS9-1, EXT-IS10-1, INT-IS6-3, INT-IS6-5, INT-IS6-7, INT-IS7-1, INT-IS7-3, INT-IS7-5, INT-IS7-7, INT-IS8-1, INT-IS8-3, INT-IS8-5, INT-IS8-7, INT-IS9-1, INT-IS9-3, INT-IS9-5, INT-IS10-3
Maximal flexion in frontal plane	Rectus abdominis Transversus abdominis External oblique	Rect-abd, TR1, TR2, TR3, TR4, TR5, E05, E06, E07, E08

Table A.2: muscles reaching maximal activation during static analysis. In the course of isometric extension analysis, muscles in lumbar region exhibit raised activation levels. Contrariwise, throughout isometric flexion analysis, abdominal muscles show elevated activation levels. For the assessment of isometric flexion in frontal plane, asymmetric activation pattern of abdominal muscles is revealed.

.

B

Dynamic analysis

B.1. Dynamic analysis: preserved muscle groups

Muscle group	Muscle subgroup	Muscle
Sacrospinalis	Longissimus thoracis pars lumborum Longissimus thoracis pars thoracis Iliocostalis lumborum par lumborum Iliocostalis lumborum par thoracis	IL1, IL2, IL3, IL4, IL-R4, IL-R6, IL-R7, IL-R8, IL-R9, IL-R10, IL-R11, IL-R12, LT-PT-T1, LT-PT-T2, LT-PT-T3, LT-PT-T4, LT-PT-T5, LT-PT-T6, LT-PT-T7, LT-PT-T9, LT-PT-T10, LT-PT-T11, LT-PT-T12, LT-PT-R4, LT-PT-R5, LT-PT-R6, LT-PT-R7, LT-PT-R9, LT-PT-R10, LT-PT-R11, LT-PT-R12, LT-PL-T1, LT-PL-T2, LT-PL-T3, LT-PL-T4
Transversospinalis	Multifidus lumborum Multifidus thoracis	MF-M1S, MF-M1T-1, MF-M1T-2, MF-M1T-3, MF-M2S, MF-M2T-1, MF-M2T-2, MF-M2T-3, MF-M3S, MF-M3T-1, MF-M3T-2, MF-M3T-3, MF-M4S, MF-M4T-1, MF-M4T-2, MF-M4T-3, MF-M5S, MF-M5T-1, MF-M5T-2, MF-M5T-3, MF-M1-laminar, MF-M2-laminar, MF-M3-laminar, MF-M4-laminar, MF-M5-laminar, Multi-L2-T12, Multi-L1-T12, Multi-T12-T10, Multi-T11-T9, Multi-T10-T8, Multi-T9-T7, Multi-T8-T6, Multi-T7-T5, Multi-T5-T3, Multi-T4-T2
External oblique	External oblique	E05, E06, E07, E08,E09, E010, E011, E012

Muscle group	Muscle subgroup	Muscle
Internal oblique	Internal oblique	IO1, IO2, IO3, IO4, IO5, IO6
Rectus abdominis	Rectus abdominis	Rect-abd
Transversus abdominis	Transversus abdominis	TR1, TR2, TR3, TR4, TR5
Psoas major	Psoas major	PS-L1-VB, PS-L1-TP, PS-L1-L2-IVD, PS-L2-TP, PS-L2-L3-IVD, P3-L2-TP, PS-L3-TP, PS-L3-L4-IVD, PS-L4-TP, PS-L4-L5-IVD, PS-L5-TP, PS-L5-VB
Quadratus laborum	Quadratus laborum	QL-post-1-L3, QL-post-2-L2, QL-post-2-L3, QL-post-2-L4, QL-post-3-L1, QL-post-3-L2, QL-mi-L3-12-3, QL-mi-12-12-2, QL-mi-12-1, QL-mi-L2-12-1, QL-mi-L4-12-3, QL-mi-L3-12-1, QL-mi-L3-12-2, QL-mi-L3-12-3, QL-ant-2-T12, QL-ant-3-T12, QL-ant-2-12-1, QL-ant-3-12-2, QL-ant-3-12-3

Table B.1: preserved muscle groups throughout dynamic analysis. Considering that focus is on lumbar stabilization, inconsequential muscles are removed from the model. Accordingly, in the course of dynamic analysis, model comprises 274 muscles.

B.2. Dynamic analysis: inertial parameters

Body	Old COM value	New COM value	Old integrator steps	New integrator steps
$\mathcal{L}4$	(0.016 0.016 0)	(0.016 0.018 0)	18	7
$\mathcal{L}5$	(0.029 0.067 0)	(0.029 0.073 0)	18	7

Table B.2: overview of modified inertial parameters. Schmid et al. [43] refined an OpenSim model for static analysis. As a consequence, inertial parameters were considered subordinate. However, in dynamic analysis, inertial parameters play a significant role. For simplicity, muscles are removed from the model and simulations of 0.1-s are executed. Finally, due implied modifications, number of integrator steps decreased by a factor 2.5.

.

B.3. Dynamic analysis: joint types

Joint	Old joint type	New joint type	Old integrator steps	New integrator steps
$\mathcal{T}11 - \mathcal{T}12$	Custom (3-DOF)	Pint (1-DOF)	7	7
$\mathcal{T}10 - \mathcal{T}11$	Custom (3-DOF)	Pint (1-DOF)	7	7
$\mathcal{T}9 - \mathcal{T}10$	Custom (3-DOF)	Pint (1-DOF)	7	7
$\mathcal{T}8 - \mathcal{T}9$	Custom (3-DOF)	Pint (1-DOF)	7	7
$\mathcal{T}7 - \mathcal{T}6$	Custom (3-DOF)	Pint (1-DOF)	7	7
$\mathcal{T}6 - \mathcal{T}5$	Custom (3-DOF)	Pint (1-DOF)	7	7
$\mathcal{T}5 - \mathcal{T}4$	Custom (3-DOF)	Pint (1-DOF)	7	7
$\mathcal{T}4 - \mathcal{T}3$	Custom (3-DOF)	Pint (1-DOF)	7	7
$\mathcal{T}3 - \mathcal{T}2$	Custom (3-DOF)	Pint (1-DOF)	7	7
$\mathcal{T}2 - \mathcal{T}1$	Custom (3-DOF)	Pint (1-DOF)	7	7
$\mathcal{T}1 - \mathcal{T}2$	Custom (3-DOF)	Pint (1-DOF)	7	7
$\mathcal{T}1 - \mathcal{R}1$	Custom (3-DOF)	Weld (0-DOF)	7	5
$\mathcal{T}2 - \mathcal{R}2$	Custom (3-DOF)	Weld (0-DOF)	7	5
$\mathcal{T}3 - \mathcal{R}3$	Custom (3-DOF)	Weld (0-DOF)	7	5
$\mathcal{T}4 - \mathcal{R}4$	Custom (3-DOF)	Weld (0-DOF)	7	5
$\mathcal{T}5 - \mathcal{R}5$	Custom (3-DOF)	Weld (0-DOF)	7	5
$\mathcal{T}6 - \mathcal{R}6$	Custom (3-DOF)	Weld (0-DOF)	7	5
$\mathcal{T}7 - \mathcal{R}7$	Custom (3-DOF)	Weld (0-DOF)	7	5
$\mathcal{T}8 - \mathcal{R}8$	Custom (3-DOF)	Weld (0-DOF)	7	5
$\mathcal{T}9 - \mathcal{R}9$	Custom (3-DOF)	Weld (0-DOF)	7	5

Table B.3: overview of modified joint types. Schmid et al. [43] incorporated custom joints characterized by 3-DOF. With the aim of enhancing computation time, ribs are welded to the spine and lumbar joints are converted to joints incorporating 1-DOF. As a consequence, lumbar spine is free to move in sagittal plane. For simplicity, muscles are removed from the model and simulations of 0.1-s are executed. Ultimately, number of integrator steps decreased by a factor 1.4.

.

B.4. Dynamic analysis: tendon slack length

Muscle	Old tendon slack length	New tendon slack length
IL-L1	0.12254	0.12554
IL-L2	0.087438	0.087638
IL-L3	0.058129	0.058149
IL-L4	0.039144	0.039194
IL-R8	0.15068	0.15168
IL-R10	0.089692	0.089693
LT-PT-T4	0.26513	0.26533
LT-PL-L1	0.10175	0.10176
MF-M1S	0.022626	0.023626
MF-M4S	0.025644	0.035644
MF-M4T-1	0.023531	0.053531
MF-M5T-2	0.021395	0.031395
MF-M5T-3	0.015271	0.025271
MF-M1-laminar	0.014219	0.014229
MF-M2-laminar	0.011814	0.011844
MF-M4-laminar	0.012644	0.012664
MF-M5-laminar	0.0083954	0.0086954
Multi-L2-T12	0.018190	0.018490
Multi-T3-T1	0.010297	0.011297
Multi-T8-T6	0.012121	0.012721
Multi-T9-T7	0.0095252	0.0097252
Multi-T12-T10	0.013115	0.016717
E05	0.0088890	0.019888
E06	0.014711	0.014741
E07	0.019239	0.019539
E08	0.021880	0.023880
E09	0.023113	0.028113
IO1	0.010436	0.010736
IO2	0.010100	0.011106
IO3	0.011100	0.013100
EXT-IS10-1	0.00094017	0.0095017
EXT-IS10-3	0.00093796	0.0093896
EXT-IS11-1	0.00093635	0.0093735
EXT-IS11-3	0.00092853	0.0094853
INT-IS10-3	0.00090942	0.0039094
INT-IS11-3	0.00094127	0.0094127
PS-L1-VB	0.15730	0.15740
PS-L1-TP	0.14711	0.15711

Table B.4: overview of modified tendon slack length. By way of expanding tendon slack length, normalized fiber velocity descends and large velocity spikes vanish. Initially, it took 4.5-h to simulate 4-s. In fullness of time, CPU reduced from 4.5-h to 30-s. From another point of view, number of integrator steps reduced from 2548 to 318.

C

Averaging techniques

C.1. Averaging across repetitions

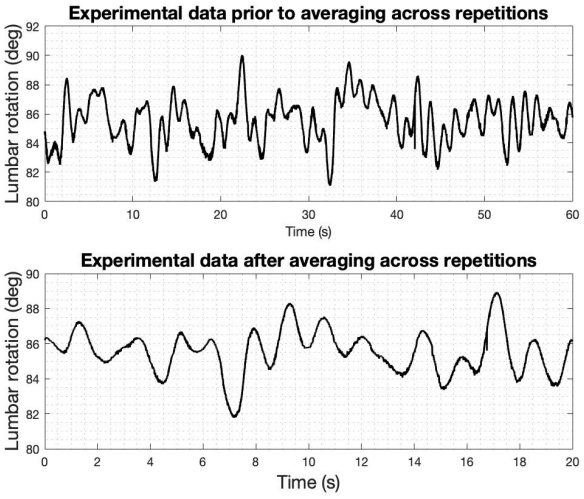

Figure C.1: impact of averaging across repetitions. *Top* figure shows unstirred data from a single participant. *Bottom* figure shows data ensuing averaging. Positive rotation is associated with lumbar flexion. Conversely, negative rotation is associated with lumbar flexion

.

C.2. Averaging across trials

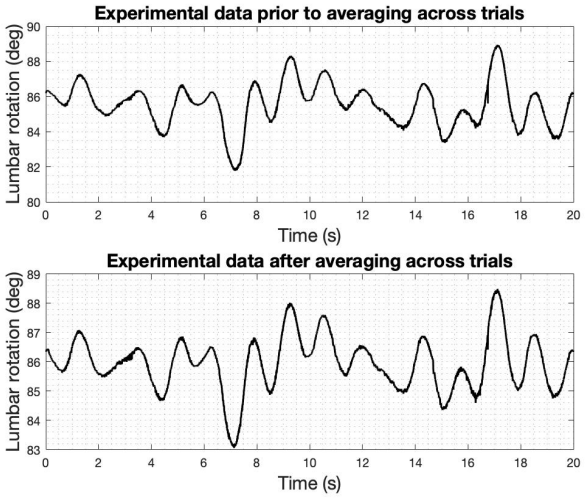

Figure C.2: impact of averaging across trials. *Top* figure expresses data from a single trial. *Bottom* figure, on the other hand, expresses data after averaging across trials. Positive rotation is associated with lumbar flexion. Conversely, negative rotation is associated with lumbar flexion

C.3. Averaging across subjects

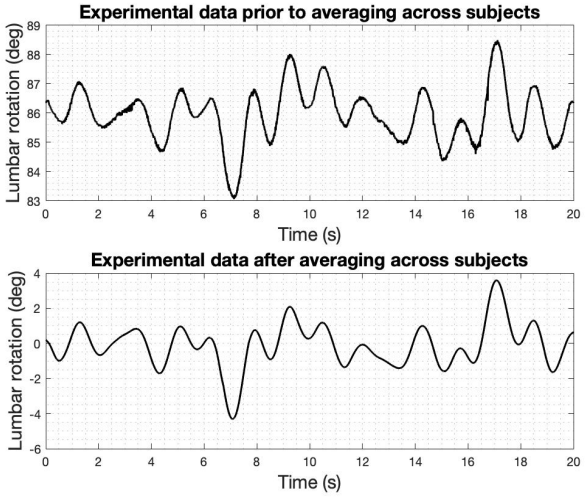

Figure C.3: impact of averaging across subjects. Prior to averaging, kinematics are centered around the zero amplitude line. *Top* figure reveals data from a single trial. *Bottom* figure, on the contrary, reveals the averaged data. Positive rotation is associated with lumbar flexion. Conversely, negative rotation is associated with lumbar flexion